Iterative Algorithms for Abundance Estimation on Unmixing of Hyperspectral Imagery

By

Samuel Rosario Torres

A thesis submitted in partial fulfillment of the requirements for the degree of

MASTER OF SCIENCE IN COMPUTER ENGINEERING

University of Puerto Rico
Mayagüez Campus
2004

Approved by:

______________________________ ____________

Shawn D. Hunt, Ph.D. Date
Member, Graduate Committee

______________________________ ____________

Néstor J. Rodríguez Rivera ,Ph.D. Date
Member, Graduate Committee

______________________________ ____________

Miguel Vélez Reyes, Ph.D. Date
President, Graduate Committee

______________________________ ____________

Fernando Gilbes, Ph.D. Date
Representative of Graduate Studies

______________________________ ____________

Jorge Ortiz Alvarez, Ph.D. Date
Chairperson of the Department

ABSTRACT

Iterative Algorithms for Abundance Estimation on Unmixing of Hyperspectral Imagery

By

Samuel Rosario Torres

Hyperspectral sensors collect hundreds of narrow and contiguously spaced spectral bands of data organized in the so-called hyperspectral cube. The spatial resolution of most Hyperspectral Imagery (**HSI**) sensors flown nowadays is larger than the size of the objects being observed. Therefore, the measured spectral signature is a mixture of the signatures of the objects in the field of view of the sensor. The high spectral resolution can be used to decompose the measured spectra into its constituents. This is the so-called *unmixing problem* in HSI. *Spectral unmixing* is the process by which the measured spectrum is decomposed into a collection of constituent spectra, or *endmembers*, and a set of corresponding fractions or *abundances*. Unmixing allows us to detect and classify subpixel objects by their contribution to the measured spectral signal. In this research, two new abundance estimation algorithms based on a least distance least square problem and compare it with other approaches presented in the literature were developed. Algorithm validation and comparison are done with real and simulated HSI data. HSI Abundance Estimation Toolbox (**HABET**) was implemented in the ENVI/IDL environment. Application of the unmixing algorithm for remote sensing of benthic habitats is presented.

RESUMEN

Separación de Imagenes Hiperespectrales usando Algoritmos Iterativos Multiplicativos

Por

Samuel Rosario Torres

Los sensores de Hyperespectral recogen centenares de estrechas y continuas bandas espectrales de datos organizados en el llamado cubo hyperspectral. La resolución espacial de la mayoría de los sensores hyperespectrales (**HSI**) que vuelan hoy en día es más grande que el tamaño de los objetos que son observados. Por lo tanto, la señal espectral medida por el sensor es una mezcla de las señales de los objetos en el campo visión del sensor. La alta resolución espectral se puede utilizar para descomponer los espectros medidos en sus componentes principales. Éste es el problema de separación en HSI. La separación espectral es el proceso por el cúal, el espectro medido por el sensor es descompuesto en una colección de espectros constituyentes, o endmembers, y un conjunto de fracciones o de abundancias correspondientes. Separación de HSI permite que detectemos y que clasifiquemos objetos del subpixel por su contribución a la señal espectral medida. En está investigación, se desarrollaron nuevos algoritmos para la estimación de abundancia basados en el problema de distancias mínimas de cuadrados mínimos y son comparados con algoritmos que se encuentra en la literatura. Validaciones y comparaciones de los algoritmos son realizados con datos hyperespectrales reales y simulados. Además, se desarollo un toolbox de estimación de abundancias HSI (**HABET** siglas en ingles) en el ambiente de programación ENVI/IDL. El uso de algoritmos de separación para la observación con satélites hiperespectrales de habitat bénticos es presentado.

ACKNOWLEDGMENTS

This work reported herein was funded primarily by the **Tropical Center for Earth and Space Studies** a **NASA URC Program** under Grant NCC5-518 and the **Air Force Research Laboratories**. The research performed here used facilities of the **Center for Subsurface Sensing and Imaging Systems** sponsored by the Engineering Research Centers Program of the US **National Science Foundation** under grant EEC-9986821.

An special Thanks to my advisor Miguel Vélez Reyes who was helping me thought my master studies.

TABLE OF CONTENTS

LIST OF TABLES

LIST OF FIGURES

CHAPTER 1

Introduction

Hyperspectral Imaging (HSI) is used for environmental monitoring and object detection. In HSI hundreds of images are taken at narrow and contiguous spectral bands providing us with high spectral resolution data that can be used to discriminate between objects based on their spectral signature [1], [2]. HSI sensors on environmental applications have high spectral resolution and low spatial resolution so that the measure spectral signature is a mixture of the spectral signatures of the objects in the field of view of the sensor [1]. An important problem in HSI processing is to decompose the mixed pixels into the materials that contribute to the pixel, *endmember* and a set of corresponding fractions of the spectral signature in the pixel, *abundances*, this problem is known as the *unmixing problem* [1], [3]. Pixel unmixing has important applications such as object quantification, mineral identification, plants health, automatic materials detection etc [3], [4]. In addition, it can be used to generate a better training set for image classification. Most approaches for unmixing perform endmember extraction and abundance estimation separately with significant human interaction, making a very interactive process such as in ENVI® Hyperspectral Image processing software. The use of iterative algorithms is investigated here to estimate the abundances of HSI.

1.1 Problem Statement

HSI sensors provide high spectral resolution order of hundreds of bands but with relative low spatial resolution. Mixed pixels are consequence of low spatial resolution of HSI sensor; the measure spectral signature is a mixture of the signatures of the objects of the field of view of the sensor [2]. In addition, mixed pixels could be as a results of different materials combined in a homogeneous mixture [3]. *Spectral unmixing* is the procedure of decompose the measure spectrum of mixed pixels into a set of originating spectra, *endmember*, and a set of corresponding abundance fractions, *abundances* [1], [3]. When any knowledge of the endmembers and the abundances is not know, the unmixing process is refered as *Full Unmixing Problem* (**FUP**). When a priory information of the endmembers is known, the process is referred as *Abundance Estimation Problem* (**AEP**). In the literature, different approaches to solve the unmixing problem are presented but most of them are based on the *Linear Mixing Model* (**LMM**) [1], [3], [5], given by:

$$\mathbf{b} = \sum_{i=1}^{n} x_i \mathbf{a}_i + \mathbf{w} = \mathbf{A}\mathbf{x} + \mathbf{w} \tag{1.1}$$

where $\mathbf{A} \in \Re_+^{m \times n}$ is the matrix of the endmember where $\mathbf{a}_i$ is the spectral signature of the i-th endmember; $\mathbf{x} \in \Re_+^n$ is the vector of the abundances; $\mathbf{b} \in \Re^m$ the measured pixel spectrum; $\mathbf{w}$ is the noise vector; n is the number of endmember and m is the number of spectral channel of the sensor [1], [3], [6]. Notice that the entries for the variables $\mathbf{A}$ and $\mathbf{b}$ are constrained to be positive in order to have physical meaning; in addition, the abundance vector need to satisfy $\mathbf{x} \geq 0$ and $\sum^n x_i \leq 1$ or $\sum^n x_i = 1$. The LMM assume that the incident light interact with the surface with only one endmember (no multiple scattering between endmembers), the total surface area is a linear combination of the abundances of the endmember as shown in the Figure 1.1 (a) [1], [3]. In other cases, the light interacts with multiples components i.e. having multiples scattering of the light produced by different objects, targets from the scene as shown in the Figure 1.2 (b). In the Figure 1.1 (b) shows the resulting mixing of the endmembers of the Figure 1.1 (a) using the LMM. In

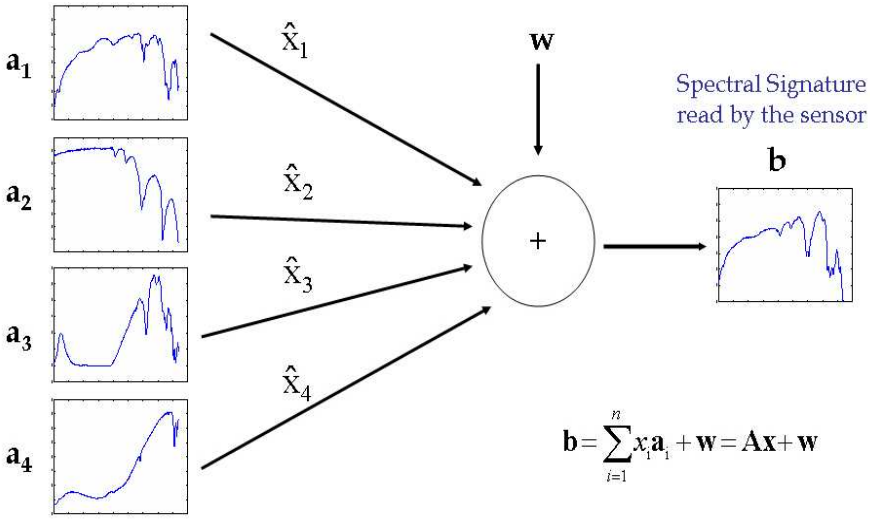

Figure 1.1: Mixed Pixel Illustration.

the literature, most of the developed algorithms for the unmixing problem don't estimate the endmember and the abundances simultaneously. They first estimate the endmembers by one of the severals methods [5], and then estimate the abundances. The abundance estimation problem (AEP) can be viewed as constrained a Distance Minimization Problem **DMP** given by:

$$\widehat{\mathbf{x}} = \mathbf{arg\ min}_x \mathbf{D}(\mathbf{b}, \mathbf{Ax}) \qquad (1.2)$$
$$\textbf{subject to } \mathbf{x} \geq 0 \textbf{ and } \sum_{i=1}^{n} x_i = 1$$

where $\mathbf{D}(\mathbf{b}, \mathbf{Ax})$ is a "distance" function, $\mathbf{A}$ is the endmember matrix, $\mathbf{b}$ is the pixel observed and $\mathbf{x}$ is the abundance vector. Different distance function lead to solutions with different properties. In this research, algorithms based on minimization of *Least Square Distance* and *Kullback-Leibler* generalized distance are studied [1], [7].

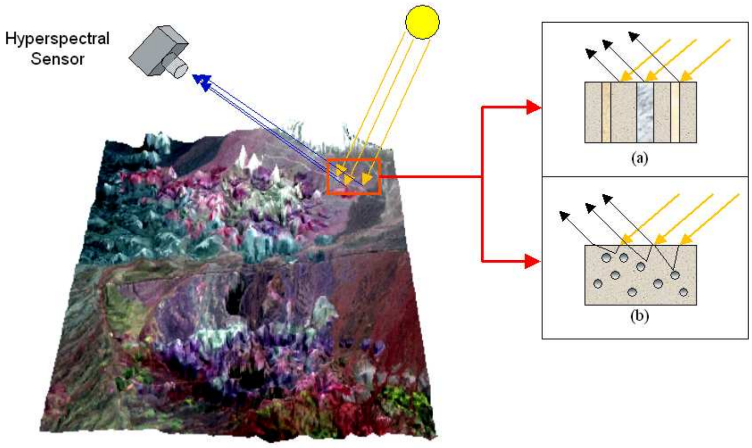

Figure 1.2: Mixing Models: (a) Linear Mixing; (b) Non-Linear Mixing.

1.2 Objectives

Main Objective

The main objective of this research was the development and the study of abundance estimation algorithms. More specific objectives were:

- Implement abundance estimation algorithms in the ENVI® environment.
- Study the abundance estimation algorithms performance under different endmembers and abundances conditions using simulate and real data.
- Comparison of developed algorithms with the methods presented in the literature.
- Develop a software tool to facilitate the use of the algorithms in ENVI.

1.3 Hyperspectral Imagery

Spectroscopy is the study of electromagnetic radiation, is derived from spectrophotometry, the measure of photons as a function of wavelength [8]. *Imaging spectroscopy* is a technique for obtaining a spectrum in each position of spatial positions (observed area) so that any one spectral wavelength can be used to make a recognizable image [8]. Imaging spectroscopy has many names in the remote sensing community, including imaging spec-

Table 1.1: HSI Sensor Characteristics

	Spectral Resolution	Spatial Resolution	Number of Bands	Spectral Range
AVIRIS	$10nm$	4-20m	224	0.4-2.45μm
HYDICE	$10nm$	1-4m	210	0.4-2.5μm
Hyperion	$10nm$	$30m$	220	0.4-2.5μm

trometry, hyperspectral, and ultraspectral imaging. A hyperspectral sensor take images at narrow and contiguous spectral band (order of hundreds of bands) providing us with high spectral resolution data [2]. Figure 1.3 shows how HSI sensor scan an area and shows how the acquired data can be represented or interpreted as a data cube. HSI data provides us with information for better discrimination of the objects and the material observed [2]. Hyperspectral data is constantly used in detection and target recognition in many environmental applications such as vegetation stress, mineral detection, etc [2]. Some examples of the HSI sensors are the Airborne Visible/Inflared Imaging Spectrometer (AVIRIS) [4], [9], Hyperspectral Digital Imagery Collection Experiment(HYDICE) [4] and Hyperion [9]. The AVIRIS sensor has a spectral resolution of $10nm$, taking 224 contiguous bands in the spectral range of $0.4\mu m$ to $2.45\mu m$, with 4-20m of spatial resolution (depending of the altitude). AVIRIS was designed by NASA Jet Propulsion Laboratory (**JPL**). The sensor capabilities of Hyperion are 220 spectral bands from $0.4\mu m$ to $2.5\mu m$ at $10nm$ spectral resolution with a $30m$ spatial resolution and was designed by NASA [9]. Hyperion is a spaceborne HSI sensor. HYDICE is an airborne sensor with 210 spectral bands covering wavelengths of $0.4\mu m$ to $2.5\mu m$ at $10nm$ resolution with $1m$ to $4m$ of spatial resolution (depending of the aircraft altitude). HYDICE was developed by Hughes Danbury Optical Systems. The Table 1.1 show a summary of the capabilities of the sensor mentioned above.

1.4 Thesis Outline

The thesis is organized as follow. In Chapter 2, the Abundance Estimator Algorithms are presented. The basic derivation of EMML, ISRA, NNLS, CLSPSTO, NNSLO and NNSTO are discussed. Chapter 3 presents the HSI Abundance Estimation Toolbox

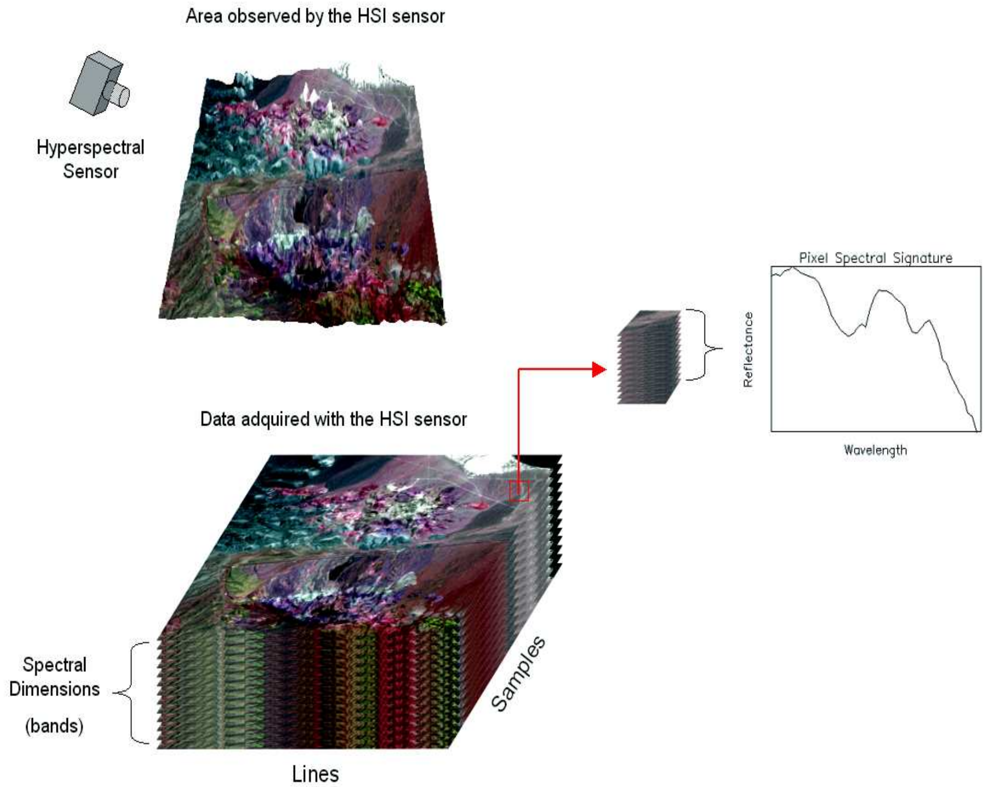

Figure 1.3: Hyperspectral Imagery Illustration.

(**HABET**). Chapter 4 presents application and performance analysis of the algorithms applied to simulated and real data. Simulated HSI data and real HSI data (Enrique Reef HSI) were used for the experiments. Chapter 5 presents the conclusions and recommendations for future work.

CHAPTER 2

Abundance Estimation Problem

In this chapter, the unmixing problem is presented as a distance minimization problem. Solutions that enforce different constraints are presented also. In all the cases, the resulting algorithm is based on solving distance minimization problem. Different algorithms based on least square and Kullback-Leibler distances are presented.

2.1 Background and Literature Review

The unmixing problem has been studied since the early days of remote sensing [6]. Solutions for this problem have confronted some limitations in the past as: limited spectral signature sampling from the targets, knowing a priori the endmembers, computational complexity plus other problems such as storage, equipment, etc [6]. With the development of hyperspectral sensors, few hundred of the *electromagnetic spectrum* at high spectral resolution are sample, in addition, with the increasing advance with computer technologies fast processing and large storage capability are accessible.

Pixel unmixing algorithms can be separate into two main areas *Endmember Determination* and *Abundance Estimation* algorithms as shown in Figure 2.1. Endmember determination methods require of a trained analyst to interaction with the algorithms or a priori information for the algorithms [3], in addition, some algorithms found in the literature use dimension reduction algorithms to reduce the data, resulting in several steps process [3], [5]. Abundances estimation methods are highly automated, little human interaction is

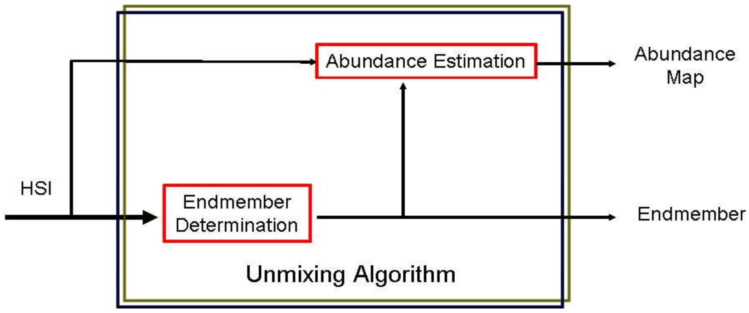

Figure 2.1: Unmixing Diagram Process

required for the algorithms to execute. The most common type of abundances estimation algorithm found, assume the endmembers are known and only estimate the abundances [3]. In the literature, unsupervised algorithms that first estimate the endmember then the abundances are found. Others algorithms found estimate both quantities simultaneously [3]. In addition, in the literature other algorithms that first estimate the endmembers and then the abundances are presented [5].

Some methods for endmember determination are Pixel Purity Index (**PPI**) integrated in the Environment Visualization Image (**ENVI**) software developed by RSI, Manual Endmember Selection Tool (**MEST**), Multiple Endmember Spectral Mixture Analysis (**MESMA**) which are describe in [5]. PPI and MEST use dimensionality reduction algorithms in order to improve performance, in PPI the dimension reduction algorithm is Minimum Noise Fraction (**MNF**) and for MEST is Principal Component Analysis (**PCA**). The PPI approach is based in geometry of convex sets and works making projection of the data sets into random vectors and counting the numbers of pixels in the extremes of the vectors, one important thing about this method is that actually do not find the last list of endmembers [5]. The MEST method has similar concepts to PPI, first reduce the dimension of the data using PCA to finds N orthogonal directions (eigenvectors) then the number of endmember to find are $N+1$, and the algorithms display the projection of N-D space of the spectral data means [5]. The main disadvantage of the PPI and MEST is dimension reduction because increase the computation time in the algorithm, also the supervise nature of the algorithms. The MESMA is based in the LMM to estimate abundances of endmembers, but this method requires extensive spectral libraries which is its main draw [5].

For abundance estimator algorithm are based on solving a DMP. The Expectation Maximization Maximum Likelihood (**EMML**) algorithm [10] used for the reconstruction of emission tomography images is used in [11] for abundance estimation. The Image Space Reconstruction Algorithm (**ISRA**) was [12] for use of image reconstruction in emission tomography in [1] present the ISRA algorithm for the use of unmixing HSI data. The EMML and ISRA algorithms are iterative algorithms, meaning that depend on the previous iteration for the next one, both algorithms guarantee the convergence and positive values in the results of the abundances. The unmixing problem normally is an overconstrained problem ($m >> n$) meanwhile in the image reconstruction problem for emission tomography is an underconstraint problem (i.e. $n > m$) [1]. The Non Negative Least Square method (**NNLS**) was introduced first in [7] by Lawson and Hanson and was used to find non negative solutions to a linear system. The NNLS algorithm is base on Active Sets Strategy, the idea of this method is if it find a negative solution x_i, set the $x_i = 0$, remove the column i from the data set re-estimate the solutions if all positive stops if not repeat the the process of setting to zero the x_i and removing the column i. The EMML, ISRA and NNLS are iterative algorithms that only satisfy the positive constraint. Chang in [13] present a series of unmixing algorithms, some of them only satisfy the sum to one constraints, also he described a full constraint algorithm for the unmixing problem. The Chang least square positive sum to one algorithms was included in this research for the comparison purpose.

2.2 Unmixing Problem

Abundance estimation is the problem of estimating the set of corresponding fractions that indicate the proportion of each endmember present in the pixel of a hyperspectral image [1], [3]. The abundance estimation problem, the endmembers are known a priori. There are different methods to obtains the endmember using algorithms such as Pixel Purity Index, ground truth or expert analysis [3], [5]. The algorithms developed in this work are based in the LMM discussed in Chapter 1.

The abundance estimation problem (**AEP**) can be view as a Distance Minimization Problem, where minimize the distance between the measured spectral response and its estimates, the LMM prediction as follows:

$$\widehat{\mathbf{x}} = \mathbf{arg\ min}_x \mathbf{D}(\mathbf{b}, \mathbf{Ax}) \tag{2.1}$$
$$\textbf{subject to } \mathbf{x} \geq 0 \textbf{ and } \sum_{i=1}^{n} x_i = 1 \textbf{ or } \sum_{i=1}^{n} x_i \leq 1$$

where $\mathbf{D}(\mathbf{b}, \mathbf{Ax})$ is a distance measure. Different algorithms presented in the literature consider none or some of the constraints. Using different distance measures would lead to different estimates. The most common distance function used in the literature is:

$$\textit{Least Square: } \mathbf{LS(Ax,b)} \ = \|Ax - b\|_2^2 \tag{2.2}$$

a second distance (actually a generalized distance [1]) studied in this research is given by:

$$\textit{Kullback-Leibler: } \mathbf{KL(Ax,b)} \ = \sum_{i=1}^{m} (\mathbf{a}_i^T \mathbf{x} \log(\frac{a_i^T x}{b_i}) + b_i - \mathbf{a}_i^T \mathbf{x}) \tag{2.3}$$

$\mathbf{LS}(\mathbf{Ax}, \mathbf{b})$ is a distance but $\mathbf{KL}(\mathbf{Ax}, \mathbf{b})$ is not a distance perse because do not satisfy the triangularity inequality [1]. An important property of both distance functions is convexity.

The next sections are presented some algorithms for the abundance estimation. In addition, the discussion of the problems inherit in each algorithms in their approach to solve the abundance estimation problem are presented.

2.2.1 Unconstrained Least Square Algorithm (ULS)

The first estimator is solution of 2.1 using the LS cost function and no constraints with is given by:

$$\widehat{\mathbf{x}}_{ULS} = (\mathbf{A}^T \mathbf{A})^{-1} \mathbf{A}^T \mathbf{b} \tag{2.4}$$

The main advantage of this approach is that it is very simple to implement and run fast. Its main disadvantage is that negatives values for the abundance could be obtained, having no physical meaning [3]. In addition, the resulting estimate may not satisfy the sum to one restriction (i.e. $\sum x_i = 1$).

2.2.2 Sum to One Only Least Square Algorithm (STOLS)

In the previous section, the direct solution algorithm for LS was presented (2.4). Direct solution of least square problem including the sum to one constraints ($\sum x_i = 1$) can be estimated. The Lagrangian function for this problem is given by:

$$L(\mathbf{x}, \lambda) = \frac{1}{2} \parallel \mathbf{Ax} - \mathbf{b} \parallel_2^2 + \lambda(\mathbf{1}^T\mathbf{x} - 1) \tag{2.5}$$

where λ is the lagrange multiplier. Deriving the $L(\mathbf{x})$ respect to $\mathbf{x}$, $\frac{\delta L(\mathbf{x},\lambda)}{\delta \mathbf{x}}$ obtain the following:

$$\begin{gathered}\widehat{\mathbf{x}}_{STO} = \widehat{\mathbf{x}}_{ULS} + (\mathbf{A}^T\mathbf{A})^{-1}\lambda\mathbf{1} \\ where\ \lambda = \frac{1 - \mathbf{1}^T\widehat{\mathbf{x}}_{ULS}}{\mathbf{1}^T(\mathbf{A}^T\mathbf{A})^{-1}\mathbf{1}}\end{gathered} \tag{2.6}$$

where, $\hat{\mathbf{x}}_{ULS}$ is the solution of the unconstraint problem (eq. 2.4) and $\mathbf{1} = [1, 1, 1, ..., 1]^T$ is a vector of ones of n dimensions. This approach still very simple to implement but the resulting abundances may be negatives resulting in a solution with no physical meaning [1], [3].

Chang Least Square Sum To One Algorithm (CLSSTO)

Other alternatives have been used by other authors as Chang to utilize least square to estimate the abundance for the desire pixel. The technique applied by Chang is know as quadratic penalty [13]. First lets define $V(\mathbf{x})$:

$$V(\mathbf{x}) = (\mathbf{b} - \mathbf{Ax})^T(\mathbf{b} - \mathbf{Ax}) + \lambda^2(1 - \mathbf{1}^T\mathbf{x})^2 \tag{2.7}$$

The idea of this technique is based on incrementing lambda to force the constraint to be satisfied. In [13], the solutions for the sum to one constraint and with full constraints are presented. Lets rewrite the 2.7 in the following form:

$$\mathbf{min}\ \|\bar{\mathbf{b}} - \bar{\mathbf{A}}\mathbf{x}\| \tag{2.8}$$

where $\bar{\mathbf{b}} = \begin{bmatrix} \mathbf{b} & \lambda \end{bmatrix}^T$ and $\bar{\mathbf{A}} = \begin{bmatrix} \mathbf{A}^T & \lambda\mathbf{1} \end{bmatrix}^T$ and λ is the weight as λ is increased the sum to one constraint is enforced. Following the same approach as with unconstraint least square (eq. 2.4) the following solution is obtained:

$$\widehat{\mathbf{x}}_{\mathbf{CSTO}} = (\bar{\mathbf{A}}^T\bar{\mathbf{A}})^{-1}\bar{\mathbf{A}}^T\bar{\mathbf{b}} = (\mathbf{A}^T\mathbf{A} + \lambda^2 I)^{-1}(\mathbf{A}^T\mathbf{b} + \lambda^2\mathbf{1}) \tag{2.9}$$

The Chang least square sum to one (CLSSTO) algorithm is described in [13]:

CLSSTO Algorithm:

1. Set $\lambda = 10000$ and set $\varepsilon = 0.001$ (ε is a value to determinate closeness to zero)
2. Compute $\hat{\mathbf{x}}_{\mathbf{CSTO}}$ from equation 2.9
3. If $\mid \mathbf{1}^T\hat{\mathbf{x}} - 1 \mid > \varepsilon$ then increase λ and go to 2
4. else $\hat{\mathbf{x}}$ is the solution.

The variable ε is set to a value close to zero the sum to one conditions is closer to one, $\sum x_i \approx 1$. In the algorithm as the value of λ increase, the sum to one constraints is enforced more strongly [13]. Similar to the algorithm (2.6) estimates with not physical meaning when may arise. The CLSSTO algorithm is the same algorithm of Linear Unmixing described in ENVI.

2.2.3 Positive Constraint Only Algorithms

In the literature, algorithms considering non negative constraints only of the equation 2.1 are founded, the simplification of problem is:

$$\widehat{\mathbf{x}} = \mathbf{arg\ min}_x \mathbf{D}(\mathbf{b}, \mathbf{A}\mathbf{x}) \tag{2.10}$$

$$\mathbf{subject\ to\ x} \geq 0.$$

Using the Lagrange function $\mathbf{L(x,u)} = \mathbf{D(b,Ax)} - \mathbf{u}^T\mathbf{x}$ and the (2.10) the optimal conditions for $\mathbf{x}$ using the Kuhn-Tucker conditions (presented in [14]) are.

$$\nabla_x \mathbf{L}(\mathbf{x}, \mathbf{u}) = \nabla_x \mathbf{D}(\mathbf{b}, \mathbf{A}\mathbf{x}) - \mathbf{u} = 0 \tag{2.11}$$

$$\textit{For j=1, 2, ..., n}\ \mathbf{u_j x_j} = \mathbf{0} \tag{2.12}$$

The optimal points $\mathbf{x}$ satisfy the equation (2.11) and (2.12). Solving for the equation (2.12) a generalized multiplicative positive algorithm is obtained:

$$\frac{\partial \mathbf{D(b,Ax)}}{\partial x_j} x_j = 0, \textit{For j=1, 2, ..., n.} \tag{2.13}$$

Having this generic multiplicative algorithms, different objective distance function as (2.2) or (2.3) can be used to derive a multiplicative iterative algorithm.

Image Space Reconstruction Algorithm (ISRA)

Using the Least Square objective function (eq. 2.2) in the derivation of the equation (2.13) obtain the following results:

$$\sum_{i=1}^{m} (\mathbf{a}_i^T \mathbf{x} - \mathbf{b}_i) a_{ij} x_j = 0 \Longrightarrow \hat{x}_j^{k+1} = \hat{x}_j^k \frac{\sum_{i=1}^m b_i a_{ij}}{\sum_{i=1}^m a_{ij} \mathbf{a}_i^T \hat{\mathbf{x}}}, \textit{ for j=i, ..., n} \tag{2.14}$$

the Image Space Reconstruction Algorithm (**ISRA**). In our case the matrix $\mathbf{A} \in \Re_+^{m \times n}$ is the endmember matrix, $\mathbf{b} \in \Re_+^m$ is the pixel in observation and $\hat{\mathbf{x}}$ is the abundance vector.

Notice from the ISRA algorithm that if the initial values of the vector $\hat{\mathbf{x}}$ as positive is remains positive if abundance reach zero is stay at zero. A general pseudo code for ISRA:

ISRA Algorithm

1. Initialize $\hat{\mathbf{x}}^0$, ϵ and ρ
2. while (error $\geq \epsilon$) and (stop $\geq \rho$) do
   (a) estimate $\hat{\mathbf{x}}$ using eq. (2.14)
   (b) error $= \| \mathbf{A}\hat{\mathbf{x}}^k - \mathbf{b} \|^2$
   (c) stop $= \| \hat{\mathbf{x}}^{k+1} - \hat{\mathbf{x}}^k \| / \| \hat{\mathbf{x}}^k \|$
3. return $\hat{\mathbf{x}}$

This pseudo code assume that $\hat{\mathbf{x}}$ is a non negative initial vector, $\mathbf{A}$ is a non negative endmember matrix. The algorithm stop when the error is less than ϵ or when the estimated abundance is very similar to the previous one (i.e. $\hat{\mathbf{x}}^{k+1}$ very similar to $\hat{\mathbf{x}}^k$), determined by ρ. Convergence for the ISRA algorithm have been proved in [1] and other works, in addition if the system $\mathbf{Ax} = \mathbf{b}$ has a solution (consistent system) the algorithm converge to the solution but in general were noise is present in the system $\mathbf{Ax} \neq \mathbf{b}$ (inconsistent system) the algorithm converge to a minimum of the distance solution of $\mathbf{LS}(\mathbf{b}, \mathbf{Ax})$.

The advantage of this algorithm is “simple” to implement in software and hardware, a vector form evaluation that with new days Digital Signal Processor could take advantage of this algorithm. The convergence rate of the ISRA is slow as is shown in the Table 4.1. Different methods can be use to accelerate the convergence rate for the ISRA algorithm. In the work of Meidunas [11], Block Iterative Method are used to speed up convergence rate of EMML. In this work, Relaxation technique to accelerate the convergence rate of ISRA were used. The ISRA accelerated (ISRAA) iterative algorithm:

$$\hat{x}_j^{k+1} = (1 - w)\hat{x}_j^k + w\hat{\mathbf{x}}_{ISRA} \tag{2.15}$$

where $\hat{\mathbf{x}}_{ISRA}$ is the basic ISRA estimation and w is the relaxation parameter, if $w > 1$ then is a overrelaxation parameter, in the case where $w < 1$ then is call underrelaxation parameter, if $w = 1$ obtain the original ISRA algorithm.

Non Negative Least Square Algorithm (NNLS)

Other iterative technique to solve the abundance estimation problem with Least Square is *Active Sets Strategy* [14]. Lawson and Hanson develop an algorithm based in active set strategy for Non Negative Least Square (NNLS) [7]. The idea behind the active set strategy is to divide the the constraint into two groups: the set acting as active ($\wp$) and the set acting as inactive set (Z) [14]. The set working as inactive, Z, would be ignore to find the solution of LS [14]. The NNLS is an simplification of the Least Square problem with Linear Inequality Constraints (**LSI**). The LSI Problem state as follow, Let $\mathbf{A} \in \Re^{m \times n}, \mathbf{b} \in \Re^{m}, \mathbf{G} \in \Re^{m \times n}, \mathbf{h} \in \Re^{m}$:

$$min \parallel \mathbf{Ax} - \mathbf{b} \parallel \text{ , } \textit{subject to } \mathbf{Gx} \ \geq \ \mathbf{h} \tag{2.16}$$

The Kuhn-Tucker Theorem for the LSI problem [7]: *An n-vector $\hat{\mathbf{x}}$ is a solution for the LSI Problem if and only if there exists an m-vector $\hat{\mathbf{y}}$ and a partitioning of integer 1 to m into subsets $\wp$ and Z such that:*

$$\mathbf{G}^T\hat{\mathbf{y}} = \mathbf{A}^T(\mathbf{A}\hat{\mathbf{x}} - \mathbf{b}) \tag{2.17}$$

$$\hat{r}_i = 0 \textit{ for } i \ \in z, \hat{r}_i > 0 \textit{ for } i \ \in \wp \tag{2.18}$$

$$\hat{y}_i \geq 0 \textit{ for } i \ \in z, \hat{y}_i = 0 \textit{ for } i \ \in \wp \tag{2.19}$$

$$\textit{where } \hat{\mathbf{r}} = \mathbf{G}\hat{\mathbf{x}} - \mathbf{h}. \tag{2.20}$$

Based only in the non negative constraints of the LSI problem, similar to (2.10) using the LS objective function, the NNLS Problem:

$$min \parallel \mathbf{Ax} - \mathbf{b} \parallel \text{ , } \mathit{subject\ to}\ \mathbf{x} \geq 0. \tag{2.21}$$

The constitution of the Kuhn-Tucker Conditions for the NNLS Problem (eq. 2.21) are [7]:

$$x_i > 0 \ \mathit{if}\ j \ \in \wp; x_i = 0 \ \mathit{if}\ j \ \in Z \tag{2.22}$$

$$w_i = 0 \ \mathit{if}\ j \ \in \wp; w_i \leq 0 \ \mathit{if}\ j \ \in Z \tag{2.23}$$

$$\mathbf{w} = \mathbf{A}^T(\mathbf{b} - \mathbf{Ax}) \tag{2.24}$$

$$\mathit{the\ solution\ is:}\ \mathbf{A}_{\wp}\mathbf{x} \cong \mathbf{b}$$

The NNLS algorithm described of Lawson and Hanson [7] as follows:

1. Let the set P = null and Z = {1,2,...,n}, $\hat{\mathbf{x}} = 0$.
2. Let w $\in \Re_n$, $w = A^T(b - Ax)$.
3. If Z is empty or max(w_i) ≤ 0 then go to 12.
4. Find t $\in$ Z such that w_t = max{w_j:j $\in$ Z}.
5. Move index t from set Z to set P.
6. Let $\mathbf{A}_P$ denote by m $\times$ n matrix defined by
   (a) Column j of $\mathbf{A}_P$ = {Column j of $\mathbf{A}$ if j $\in$ P or $\mathbf{0}$ if j $\in$ Z}
   (b) Compute $\mathbf{z}$ as solution of the least square problem $\mathbf{A}_P\mathbf{z} \cong \mathbf{b}$
   (c) Set $z_j = 0$ if j $\in$ Z
7. If $\hat{x}_j > 0$ $\forall$j in P set $\hat{\mathbf{x}} = \mathbf{z}$ and go to step 2
8. Find index $q \in P$ such that $\hat{x}_q/(\hat{x}_q - z_q) = min\{\hat{x}_j/(\hat{x}_j - z_j) : z_j \leq 0, j \in P\}$
9. Set $\alpha = \hat{x}_q/(\hat{x}_q - z_q)$
10. Set $\hat{\mathbf{x}} = \hat{\mathbf{x}} + \alpha(\mathbf{z} - \hat{\mathbf{x}})$

11. Remove from the set P and add to the set Z all j $\in$ P where $x_j = 0$ and go to step 6

12. End Algorithm

13. $\hat{\mathbf{x}}$ is the solution of the NNLS

The convergence of the NNLS algorithm has been proven in [7]. Is shown in [7] the maximum number of iterations for the NNLS is n, the number of endmembers.

Expectation Maximization Maximum Likelihood Algorithm (EMML)

Similar to previous section, the Kullback-Leibler objective distance function is used into the equation (2.13) to obtain the EMML iterative multiplicative algorithm:

$$\sum_{i=1}^{m}(1 - \frac{b_i}{\mathbf{a}_i^T \mathbf{x}})a_{ij}x_j = 0 \Longrightarrow \hat{x}_j^{k+1} = \hat{x}_j^k \frac{\sum_{i=1}^m (\frac{b_i a_{ij}}{\mathbf{a}_i^T \hat{\mathbf{x}}})}{\sum_{i=1}^m a_{ij}}, \textit{ For i=1, ..., } n \tag{2.25}$$

The EMML algorithm have the property if the initial values of $\mathbf{x}$ are positive its remains positive, in addition it converges to a the minimum distance solution [1]. A pseudo code for the EMML algorithm:

1. Initialize $\hat{\mathbf{x}}^0$, ϵ and ρ

2. while (error $\geq \epsilon$) and (stop $\geq \rho$) do

   (a) estimate $\hat{\mathbf{x}}$ using eq. (2.25)

   (b) error $= KL(\mathbf{A}\hat{\mathbf{x}}, \mathbf{b})$

   (c) stop $= \parallel \hat{\mathbf{x}}^{k+1} - \hat{\mathbf{x}}^k \parallel / \parallel \hat{\mathbf{x}}^k \parallel$

3. return $\hat{\mathbf{x}}$

In addition, similar to ISRA this algorithm is "simple" to implement in software and hardware, a vector form evaluation that with DSP could take advantage of this algorithm.

Using the relaxation technique presented in the previous section, the EMML accelerated algorithm (EMMLA) is obtained:

$$\hat{x}_j^{k+1} = (1 - w)\hat{x}_j^k + w\hat{\mathbf{x}}_{EMML} \tag{2.26}$$

where w is the relaxation parameter and $\hat{\mathbf{x}}_{EMML}$ is the basic EMML estimation. Similar to the ISRA pseudo code, assume that $\hat{\mathbf{x}}$ is a non negative vector, $\mathbf{A}$ is a non negative endmember matrix. The algorithm stop when the error is less than ϵ or when the estimated abundance is very similar to the previous one (i.e. $\hat{\mathbf{x}}^{k+1}$ very similar to $\hat{\mathbf{x}}^{k}$), determined by ρ.

2.2.4 Fully Constrainted Algorithms

Non-Negative Sum Less or Equal to One (NNSLO)

When enforcing the sum-to-one and the non negative constraints algorithms with both constraints doesn't consider the dark pixels as possible spectral signature obtained by a hyperspectral sensor. To include the dark pixels other type of constraints is used, sum less or equal to one to find solutions to the unmixing problem. Using the sum less or equal to one and non negative constraints the problem to solve is the following:

$$\mathbf{min}\|\mathbf{Ax}-\mathbf{b}\| \ \textit{subject to}\ \mathbf{x}\geq 0\ \textit{and}\ \mathbf{1}^T\mathbf{x}\leq 1. \tag{2.27}$$

Lets transform equation (2.27) to a Least Distance Problem (**LDP**) [7]. First, let:

$$\mathbf{Q}^T\mathbf{A} = \begin{bmatrix} \mathbf{R} \\ 0 \end{bmatrix}; \mathbf{c} = Q^T b = \begin{bmatrix} \mathbf{c}_1 \\ \mathbf{c}_2 \end{bmatrix}$$

be the QR decomposition of $\mathbf{A}$. Using the matrix $\mathbf{Q}$ and $\mathbf{R}$ from the QR decomposition and rewriting equation (2.27) as follows:

$$min\ \|\mathbf{Rx}-\mathbf{c}_1\|\ \textit{subject to}\ \mathbf{x}\geq 0, \mathbf{1}^T\mathbf{x}\leq 1 \tag{2.28}$$

Notice that $\widehat{\mathbf{x}}_{ULS} = \mathbf{R}^{-1}\mathbf{c}_1$. Define:

$$\mathbf{z} = R\widehat{\mathbf{x}} - \mathbf{c}_1 \Rightarrow \widehat{\mathbf{x}} = \mathbf{R}^{-1}(\mathbf{z} + \mathbf{c}_1) = \mathbf{R}^{-1}\mathbf{z} + \widehat{\mathbf{x}}_{ULS} \tag{2.29}$$

Substituting the equation (2.29) in the equation (2.28) obtain the following:

$$min\ \|\mathbf{z}\|\ subject\ to\ \mathbf{Gz} \geq \mathbf{g} \tag{2.30}$$

where $\mathbf{G} = \begin{bmatrix} I & -\mathbf{1} \end{bmatrix}^T \mathbf{R}^{-1}$, $\mathbf{g} = \begin{bmatrix} -\widehat{\mathbf{x}}_{ULS}^T & \mathbf{1}^T\widehat{\mathbf{x}}_{ULS} - 1 \end{bmatrix}^T$, $I \in \Re^{n\times n}$ is the identity matrix and $\mathbf{1}^T = (1\ 1\ ...\ 1)$. This is called a least distance problem (**LDP**) in [7]. Now that the original problem (eq. 2.27) was transformed to an LDP (eq. 2.30), the Theorem 5.2.1 from [15] that is proven in [7] to solve the LDP as a Non Negative Least Square Problem (eq. 2.21) can be used. An state as follow: Considering the least distance problem 2.30, let $\mathbf{u}$ be the solution to the non negative constraint problem (**NNLSP**):

$$min_u\ \|\mathbf{Eu} - \mathbf{f}\|\ subject\ to\ \mathbf{u} \geq 0, \tag{2.31}$$

where $E = \begin{bmatrix} \mathbf{G}^T & \mathbf{g}^T \end{bmatrix}^T$, $f = \begin{bmatrix} \mathbf{0} & 1 \end{bmatrix}^T$ ($\mathbf{0} = (0\ 0\ ...\ 0)$ vector of n zeros. Let $\mathbf{r} = \mathbf{Eu} - \mathbf{f}$, if $\|\mathbf{r}\| = 0$ there are no solution (i.e $\mathbf{Gx} \geq \mathbf{g}$ is inconsistent), else the vector $\mathbf{z}$ is defined as: $\widehat{\mathbf{x}} = \widehat{\mathbf{x}}_{ULS} - \mathbf{R}^{-1}\mathbf{z}$ where $z_i = -r_i/r_{n+1}$, for $1 \leq i \leq n$ and is the unique solution to (2.30), hence, the estimate of $\widehat{\mathbf{x}}$ can be done using equation (2.29).

A new algorithm based of the problem 2.27 was presented, using the results 2.30 and 2.31 the sum less or equal to one algorithm (**NNSLO**) for abundance estimation:

Algorithm NNSLO LS

1. Compute a QR decomposition of $\mathbf{A}$, $\mathbf{A} = \mathbf{Q}\begin{bmatrix} \mathbf{R} \\ 0 \end{bmatrix}$, compute $\mathbf{c} = \mathbf{Q}^T\mathbf{b} = \begin{bmatrix} \mathbf{c}_1 \\ \mathbf{c}_2 \end{bmatrix}$.
2. Compute $\widehat{\mathbf{x}}_{ULS} = \mathbf{R}^{-1}\mathbf{c}_1$

3. Set $\mathbf{G} = \begin{bmatrix} I & \mathbf{1} \end{bmatrix}^T$

4. Set $\mathbf{f} = \begin{bmatrix} \mathbf{0} & 1 \end{bmatrix}^T$

5. Set $\mathbf{g} = \begin{bmatrix} -\widehat{\mathbf{x}}_{ULS}^T & \mathbf{1}^T\widehat{\mathbf{x}}_{ULS} - 1 \end{bmatrix}^T$

6. Set $\mathbf{E} = \begin{bmatrix} \mathbf{G}^T & \mathbf{g}^T \end{bmatrix}^T$

7. Set $\mathbf{r} = \mathbf{Eu} - \mathbf{f}$, where $\mathbf{u}$ is the solution of the NNLS problem 2.31 $\mathbf{E}$, $\mathbf{f}$

8. Set $\hat{\mathbf{z}} = \{-r_i/r_{n+1}\}, 1 \leq i \leq n$

9. $\widehat{\mathbf{x}} = \widehat{\mathbf{x}}_{ULS} + \mathbf{R}^{-1}\hat{\mathbf{z}}$

The NNSLO LS algorithm solves the unmixing problem when dark pixels are considered, satisfying the non negative and sum less or equal to one constraints. Notice that NNLS problem can be solved with any of the algorithms introduced previously of NNLS.

Non Negative Sum To One (NNSTO)

Based on NNSLO algorithm a new algorithm considering non negative and sum to one constraints was derived. First let modify the (2.1) as follows:

$$\textbf{min } \|\mathbf{Ax} - \mathbf{b}\| \textbf{ subject to } \mathbf{x} \geq 0 \textbf{ and } x_1 = 1 - \sum_{i=2}^{n} x_i \tag{2.32}$$

Now lets transforms equation (2.32) to a inequality constrained problem:

$$\textbf{min } \|\overline{\mathbf{A}}\overline{\mathbf{x}} - \overline{\mathbf{b}}\| \textbf{ subject to } \overline{\mathbf{x}} \geq 0, \mathbf{1}^T\overline{\mathbf{x}} \leq 1 \tag{2.33}$$

where $\overline{\mathbf{x}} = [x_2, ..., x_n]^T$, $\overline{\mathbf{A}} = [\mathbf{a}_2 - \mathbf{a}_1, ..., \mathbf{a}_n - \mathbf{a}_1]$ and $\overline{\mathbf{b}} = \mathbf{b} - \mathbf{a}_1$. The equation (2.33) can be solve with NNSLO to estimate $\overline{\mathbf{x}}$ and $x_1 = 1 - \mathbf{1}^T\overline{\mathbf{x}}$. In this new algorithm, the sum to one and non negative constraints are satisfied, also solving the abundance estimation in this fashion the possibility of dark pixels are considered.

The new algorithm for the problem (2.32) based on NNSLO, the NNSTO LS for abundance estimation with all constraints:

Algorithm NNSTO LS

1. Set $\overline{\mathbf{A}} = [\mathbf{a}_2 - \mathbf{a}_1, ..., \mathbf{a}_n - \mathbf{a}_1]$ and $\overline{\mathbf{b}} = \mathbf{b} - \mathbf{a}_1$
2. Estimate $\overline{\mathbf{x}}$ using the NNSLO algorithm
3. $\widehat{\mathbf{x}} = \begin{bmatrix} (1 - \mathbf{1}^T \overline{x}) & \overline{\mathbf{x}}^T \end{bmatrix}^T$

The convergence of this algorithm was proven in [7]. The NNSTO algorithm solve the unmixing problem when dark pixels are considered, in addition satisfying the non negative and sum to one constraints.

Chang's Least Square Fully Constrainted (CLSPSTO)

In a similar fashion of the CLSSTO algorithm, Chang use quadratic programming to include the non negative constraints in the solution. However, the problem that Chang is solving is given by:

$$min_{\mathbf{x}}\{(\mathbf{b} - \mathbf{A}\mathbf{x})^T(\mathbf{b} - \mathbf{A}\mathbf{x})\} \ \textit{subject to} \ \mathbf{1}^T\mathbf{x} = 1 \ \textit{and} \ sign(\mathbf{x})^T\mathbf{x} = 1 \tag{2.34}$$

where sign(x) $= \frac{x_i}{|x|}$ if $x_i \neq 0$ or 0 if $x_i = 0$. Including the combination of the $\mathbf{1}^T\mathbf{x} = 1$ and $sign(\mathbf{x})^T\mathbf{x} = 1$ in the derivation of the solution guarantee the sum to one and non negative constraint [13]. The quadratic penalty function is given by:

$$V(\mathbf{x}) = (\mathbf{b} - \mathbf{A}\mathbf{x})^T(\mathbf{b} - \mathbf{A}\mathbf{x}) + \lambda_1^2(1 - \mathbf{1}^T\mathbf{x})^2 + \lambda_2^2(1 - sign(\mathbf{x})^T\mathbf{x})^2 \tag{2.35}$$

Which Chang's solve as a linear least square problem:

$$\mathbf{min} \ \|\bar{\mathbf{b}} - \bar{\mathbf{A}}\mathbf{x}\| \tag{2.36}$$

where $\widehat{\mathbf{b}} = \begin{bmatrix} \mathbf{b}^T & \lambda_1 & \lambda_2 \end{bmatrix}^T$, $\widehat{\mathbf{A}} = \begin{bmatrix} \mathbf{A}^T & \lambda_1\mathbf{1} & \lambda_2\mathbf{1} \end{bmatrix}^T$, λ_1 and λ_2 are the weight to force the sum to one and non negative constraints respectively. Similar to unconstraint least square, the direct solution to equation (2.36):

$$\widehat{\mathbf{x}}_{CLSPSTO} = (\bar{\mathbf{A}}^T\bar{\mathbf{A}})^{-1}\bar{\mathbf{A}}^T\bar{\mathbf{b}} \tag{2.37}$$

Chang's least square fully constrained algorithm is given by (CLSPSTO):

CLSPSTO Algorithm

1. Set $\lambda_1 = 10000$, $\lambda_2 = 10000$, $\varepsilon_1 = 0.01$ and $\varepsilon_2 = 0.01$.
2. Compute $\widehat{\mathbf{x}}_{CLSPSTO}$ using eq. (2.37).
3. If not all $\widehat{\mathbf{x}}_{CLSPSTO}$ are non negative remove the signature $\bar{\mathbf{a}}_i$ from $\bar{\mathbf{A}}$ or set $\bar{\mathbf{a}}_i = \bar{\mathbf{a}}_i * 10000$ if $(\widehat{\mathbf{x}}_{CFC})_i$ has the most negative value.
4. If $\mid \mathbf{1}^T\widehat{\mathbf{x}}_{CLSPSTO} - 1 \mid > \varepsilon_1$ then increase λ_1 and if $\mid sign(\widehat{\mathbf{x}}_{CLSPSTO})^T\widehat{\mathbf{x}}_{CLSPSTO} - 1 \mid > \varepsilon_2$ then increase λ_2 and go to step 2.

   Else $\widehat{\mathbf{x}}_{CLSPSTO}$ is the solution.

Increasing the value of λ_1 force the sum to one restriction and increasing λ_2 force the non negative values [13]. Convergence of this algorithm has not been shown.

2.3 Conclusions

In this Chapter, different iterative algorithms for the abundance estimation problem were presented. Solutions to the AEP with no constraints, sum to one only, positive only, positive with sum less or equal to one and positive with sum to one constraints were studied. In addition, properties of the algorithms such as convergence.

CHAPTER 3

HSI Abundance Estimator ToolBox (HABET)

In this Chapter, the HSI Abundance Estimator Toolbox (**HABET**) graphical user interface (**GUI**) to facilitate the use of the developed abundance estimation routines presented in this research is described. The interface was developed in ENVI/IDL and runs in versions greater than 3.6 and 5.6 respectively.

3.1 HABET Main Images Routines Description

The main purpose of designing a toolbox in ENVI/IDL is to facilitate the use and interaction with the processing HSI data using the abundance estimation algorithms presented in this research. In addition, developing the routines under the ENVI/IDL environment give the advantage of using the vast routines of ENVI for HSI data processing. Figure 3.1 shows the way that HABET interacts with the HSI data and the abundance estimation routines, the toolbox gets the HSI data form memory (i.e. disk or virtual memory) and the toolbox transfers it to the selected abundance estimation routine to produce the abundance estimate maps. The abundance estimation routines included in the toolbox are shown in the Figure 3.1. The process abundance estimation is shown in the Figure 3.2, first the user using the toolbox select the HSI data to be processed (Phase 1), once having the HSI data the user select the endmembers data corresponding to the HSI data (Phase 2) and finally the user select the abundance estimation method to generate the abundance image map (Phase 3).

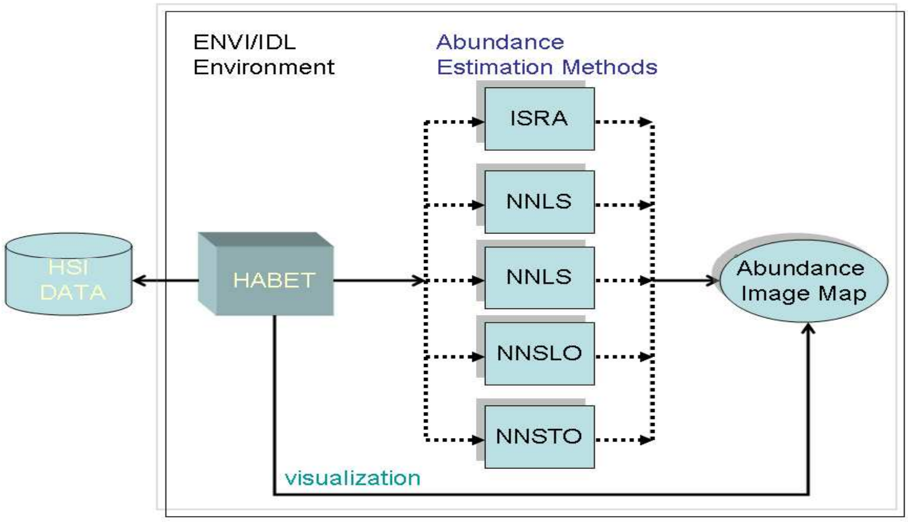

Figure 3.1: HABET Data Flow

The main routines for abundance estimation of this toolbox are shown in Figure 3.1, these are ISRA, NNLS, EMML, NNSLO and NNSTO. The ISRA algorithm was implemented similar as presented the section 2.2.3 of Chapter 2, this routine assumes that the endmembers are in $\Re_{+}^{m\times n}$ and the HSI data are in $\Re_{+}^{k\times m}$ (k is number of pixels), this routine returns an abundance estimation map. The NNLS algorithm used a routine downloaded from the web (http://hesperia.gsfc.nasa.gov/~schmahl/nnls/index.html) which is an implementation based on the algorithm described in section 2.2.3, this routine was wrapped with other routine to facilitate its use and passing fewer arguments than in the original written code and making it more similar to the other methods implemented. NNLS algorithm have the same assumptions as ISRA. The EMML algorithm have the same assumptions as ISRA also described in the section 2.2.3 of Chapter 2. NNSLO algorithm was implemented as the algorithm described in section 2.2.4, have the same assumption as ISRA.

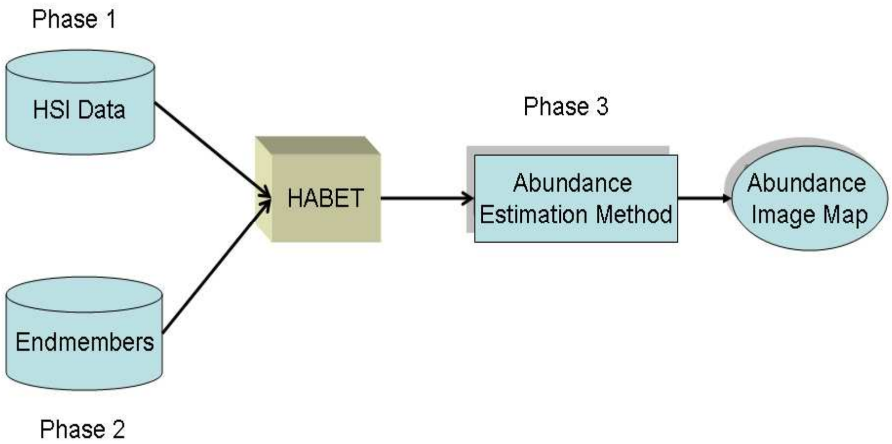

Figure 3.2: HABET Abundance Estimation Process

To implement this routine, a QR method for rectangular matrices have to be used, a QR method from the web (http://astrog.physics.wisc.edu/∼craigm/idl/math.html) was downloaded due IDL does not have a QR method for rectangular matrices implemented, also have the same assumptions as ISRA. The NNSTO algorithm was developed as described in the section 2.2.4. In this algorithm, the similar QR problem as NNSLO is confronted and use the same QR method used for NNSLO also this method have the same assumptions as ISRA. The routines implemented return an abundance estimation map of the given HSI data and the corresponded endmembers. To run this toolbox the user only type UnmixingHSIGUI (name of the main gui routine) in the command prompt of IDL and close similar as common types of windows in the x button (or selecting exit under file menu).

3.2 HABET ToolBox

The HSI Abundance Estimator ToolBox (**HABET**) includes some basic operations to facilitate the users to use the abundance estimation routines, for example: open HSI files, showing images, data information. Figure 3.3, shows the main GUI of HABET, three regions identified, Region 1, Region 2 and Region 3 are image display area, files opened

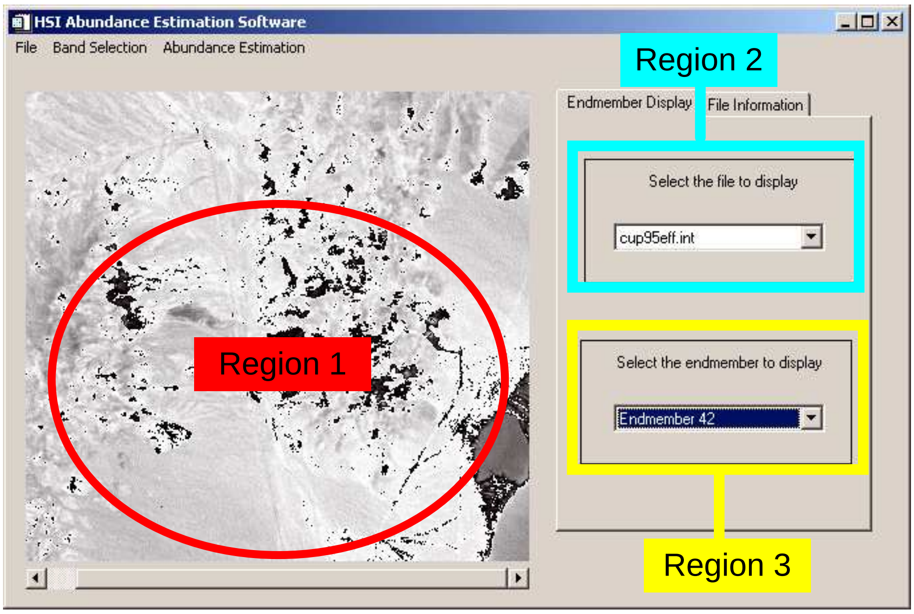

Figure 3.3: HSI Abundance Estimation ToolBox Main GUI

and endmembers (or bands) of the selected open file respectively. The user first select the file to later select the endmember to be displayed, i.e. selecting an option form the drop list menu, this update the endmember drop list menu corresponding to the selected file and the users can select endmember to be displayed form the endmember drop list menu. Figure 3.4 shows a sample of the menu options for abundance estimation, separated into two classification: positive estimators where only considers the non negative constraints and Positive with Sum to one where considers in addition of non negative, sum to one or sum less or equal to one constraints. Figure 3.5 and Figure 3.6 are the gui's to obtain the HSI data and the endmembers. The interface are similars, Region 1 is where the users can select the HSI data or the endmembers in case if the data was previously opened else the users can open the corresponding data with the associate button in the Region 2, open file. Figure 3.7 shows the tab of files information, the user selecting a file from Region 1 it show the corresponding file information in Region 2. HABET will require further testing for analysis and bugs corrections.

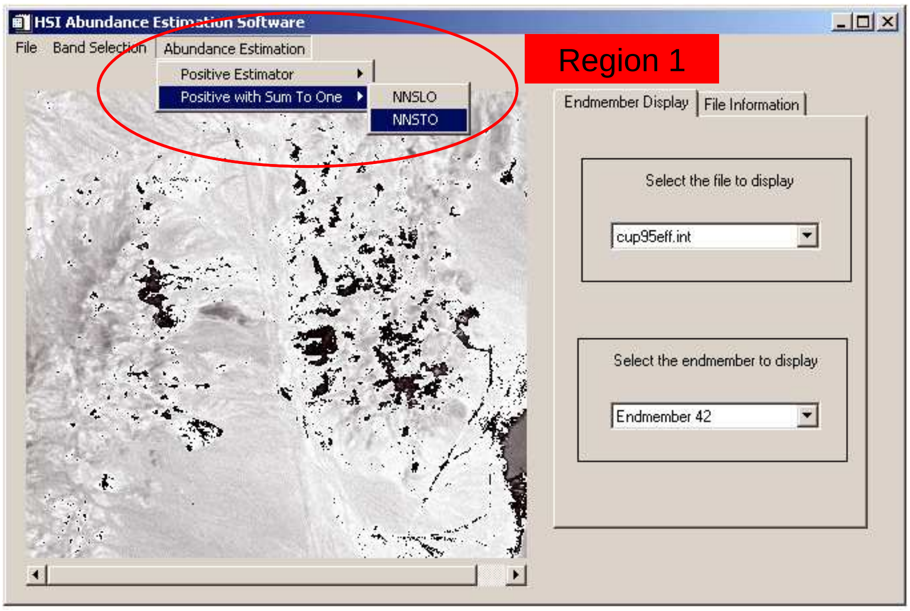

Figure 3.4: Abundance Estimation Organization Menu

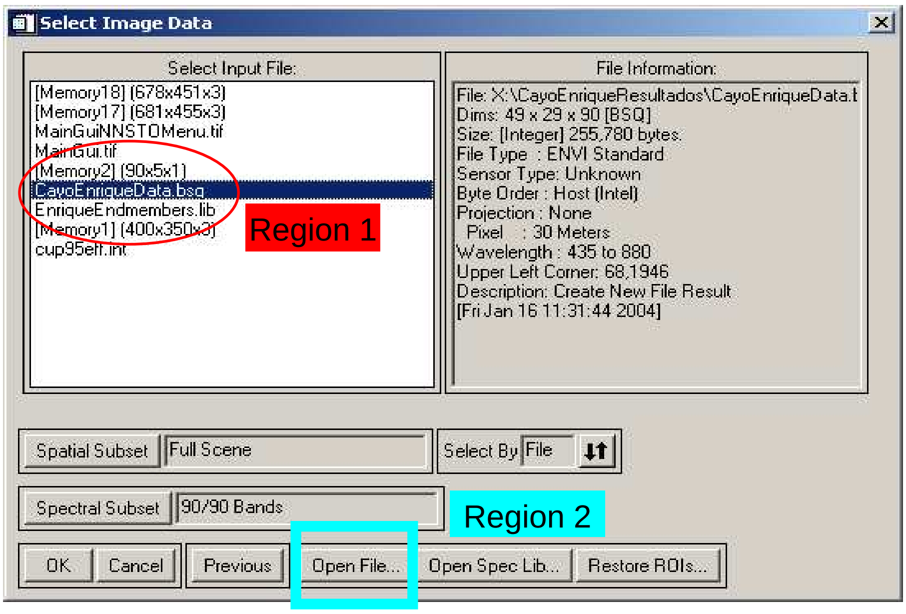

Figure 3.5: Open and File Selection GUI

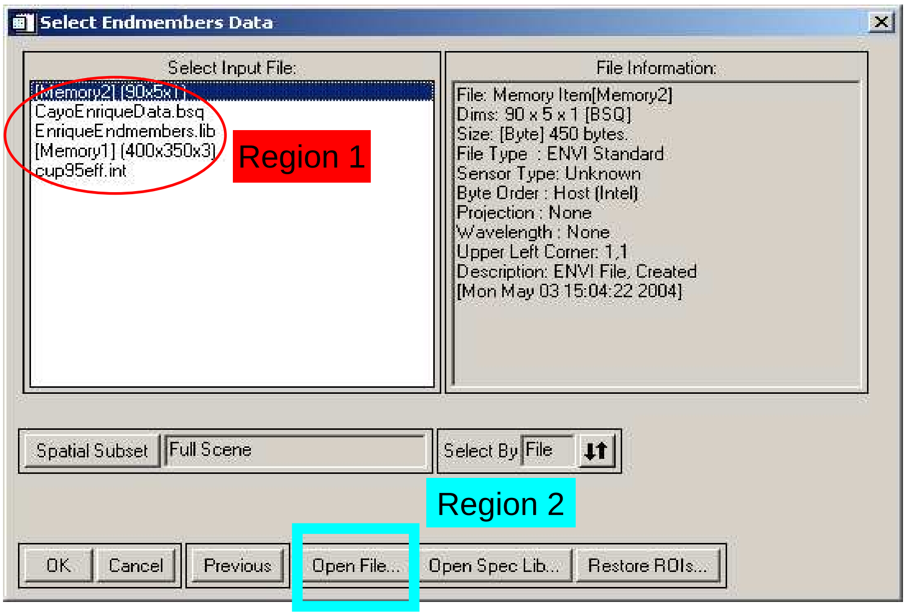

Figure 3.6: Open and Endmember Selection GUI

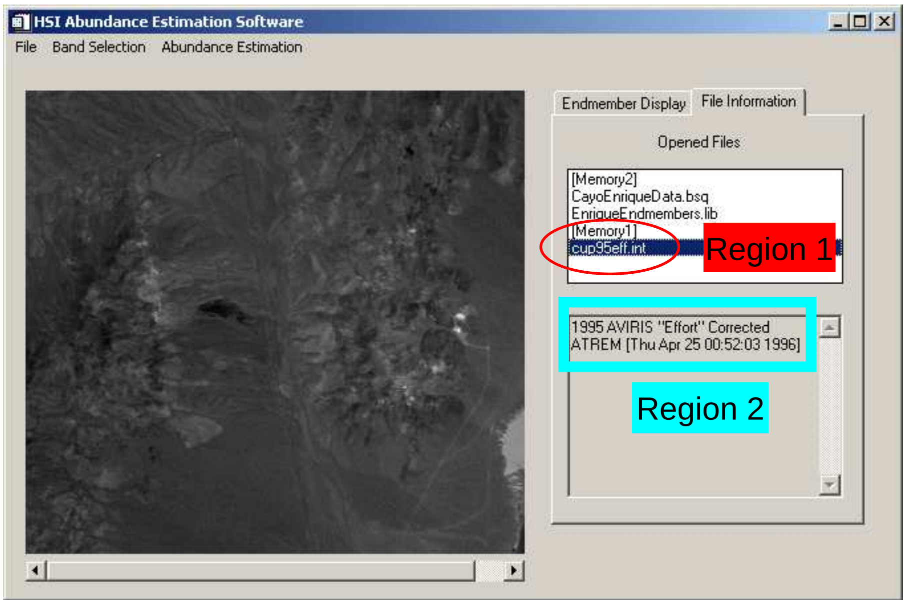

Figure 3.7: File Information

In this Chapter, the HSI Abundance Estimator ToolBox (**HABET**) were presented. Description of the main routines as ISRA, NNLS, EMML, NNSLO, NNSTO were presented. In addition, the interaction of HABET between the routines and the HSI data and the windows of selecting the HSI data and endmembers were presented.

CHAPTER 4

Algorithms Analysis and Validation

In this chapter, real and simulated HSI data is used to test and compare the abundance estimation algorithms, introduced previously. Synthetic data was generated using endmembers from the U.S. Geological Survey (**USGS**) spectral data base and the web. The HSI data used for the validation of the algorithms is taken by Hyperion HSI sensor in the La Parguera area. The routines implemented were in Environment for Image Visualization (**ENVI**) that run under Iterative Definition Language (**IDL**) version 3.5 and 5.5 respectively. The simulations were run in a Pentium 4 machine with 2.2Ghz and 1GB of RAM running Windows XP Operative System.

The results shown in the Tables 4.1-4.4 are generated averaging the results of every band for each algorithm. The results for each band is the average of eleven repetitions of abundance estimations (for time, iterations, time/iterations). The leafs synthetic data consists of a pixel of 2151 bands. The number of bands used for leafs each experiments are: 2151, 215, 107, 71, 53, 43, 35, 30, 26, 23, 21, 19, 17, 16, 15, 14, 13, 12, 11, 10, 9, 8, 7, 6, 5. The minerals synthetic data consists of a pixel of 420 bands. The number of bands used for minerals experiments are: 420, 210, 140, 105, 84, 70, 60, 52, 42, 30, 20, 15, 10, 8, 7, 6, 5. The overrelax parameter used for the leafs was 13 and for minerals was 3.5. These parameter were determined by trial and error. The implementation of the ISRA, ISRAA, NNLS, EMML and EMMLA algorithms where include a normalization (i.e. $\hat{\mathbf{x}} = \hat{\mathbf{x}}/\mathbf{1}^T\hat{\mathbf{x}}$) in trial and error test shown better convergence rate.

4.1 Synthetic Data Experiments

The experiments consists in estimating the abundance of a synthetic mixed pixel using the algorithms: EMML, EMMLA, ISRA, ISRAA, NNLS, NNSLO, NNSTO and CLSPSTO. The purpose of this experiment is to determinate which algorithms converge faster and find a reasonable abundance estimate. Synthetic HSI pixel was created using know endmembers and generating a positive random distributed abundance vector $\mathbf{x}$.

4.1.1 Experiment 1: Similar Spectral Signature

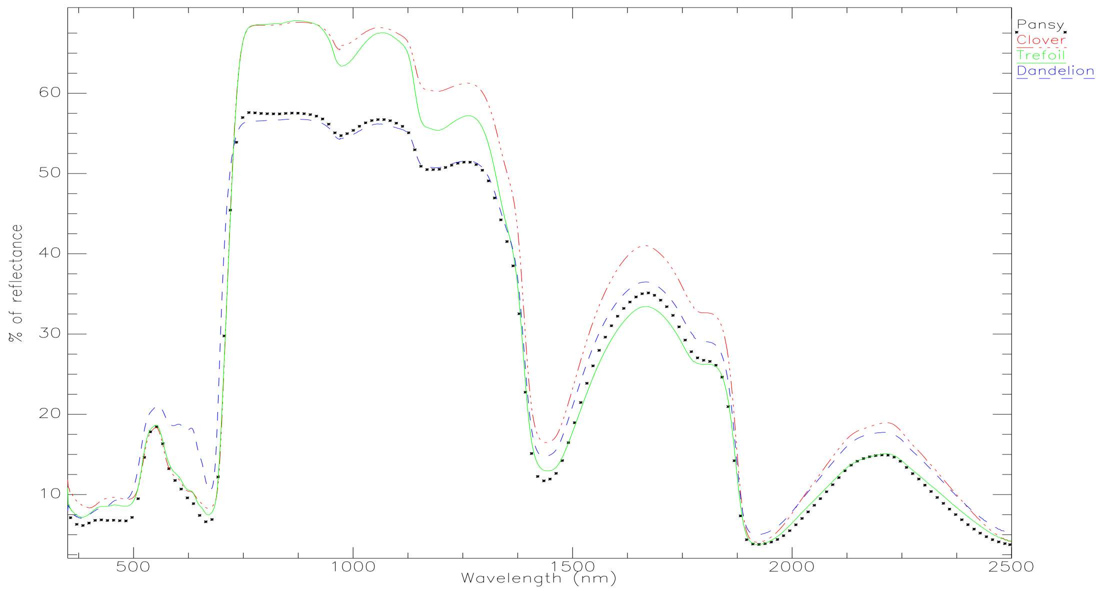

Figure 4.1: Leaf Endmembers

The first experiment consists in abundance estimation with similar spectral signatures for the endmembers. The leafs endmembers used for the experiments are: dandelion, trefoil, pansy and clover. The spectral signature of the leafs endmembers shown in the

Figure 4.1. The leafs endmembers data has 2151 bands from 350-2500nm. The abundances for each the the leafs are: Clover 0.12578, Trefoil 0.134351, Pansy 0.554631 and Dandelion 0.185238. The resulting mixed pixel used for the experiment is shown in the Figure 4.2.

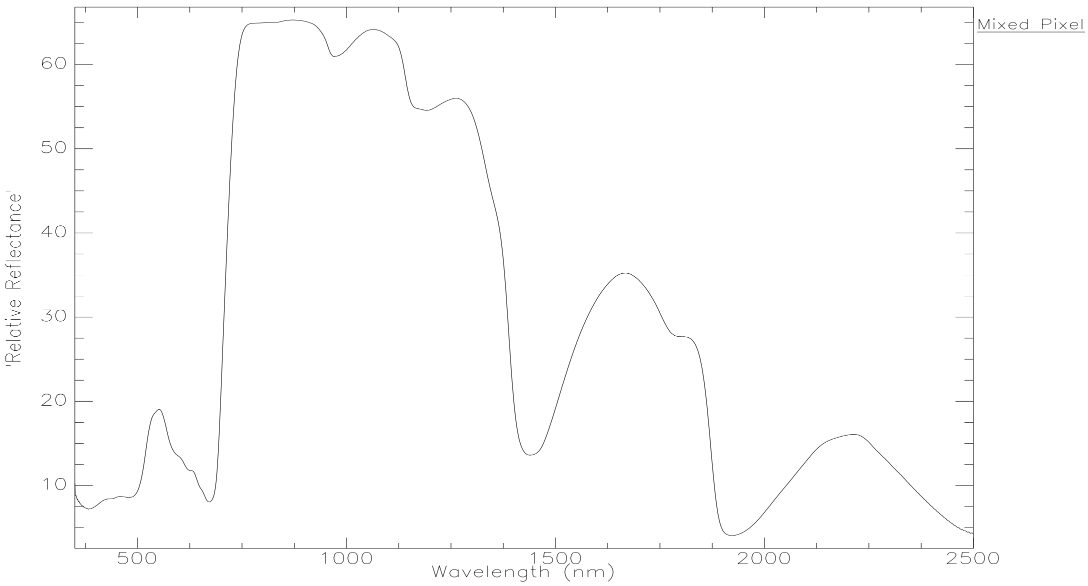

Figure 4.2: Mixed Pixel using Leafs Endmember

The timing results of the algorithms are presented in the Table 4.1. As it shows, the CLSPSTO algorithm converge faster than the others also the NNSLO is in the same order of magnitude. CLPSTO took one iteration to find the solution similar to NNSLO and NNSTO. In addition, the time by iterations of the ISRA is faster but with the same order of magnitude of ISRAA and EMML (10^{-5}).

Table 4.1: Timing Results for Leafs HSI Data (without noise)

	EMML	ISRA	EMMLA	ISRAA	NNLS	CLSPSTO	NNSLO	NNSTO
Time (sec)	10.0E-2	8.47E-2	2.58E-2	3.54E-2	3.01E-3	**1.09E-4**	6.76E-4	1.35E-3
Avg.♯ Iterations	1.07E+3	1.41E+3	2.77E+2	5.63E+2	4	**1**	**1**	**1**
Time(sec) Iterations	8.55E-5	**6.06E-5**	19.26E-5	6.31E-5	75.27E-5	10.91E-5	67.64E-5	135.3E-5

4.1.2 Experiment 2: Similar Spectral Signature with Noise

The second experiment consists in adding noise to the leafs mixed pixel to estimate the abundances. The idea behind of this experiment is to simulate an pixel more similar to the pixel taken by a HSI sensor. The noise added is Gaussian Noise with $N(0, \alpha^2 I)$ where α is the 1 percent of $max_i|b_i|$ (of the original mixed pixel). The resulting pixel is shown in the Figure 4.3.

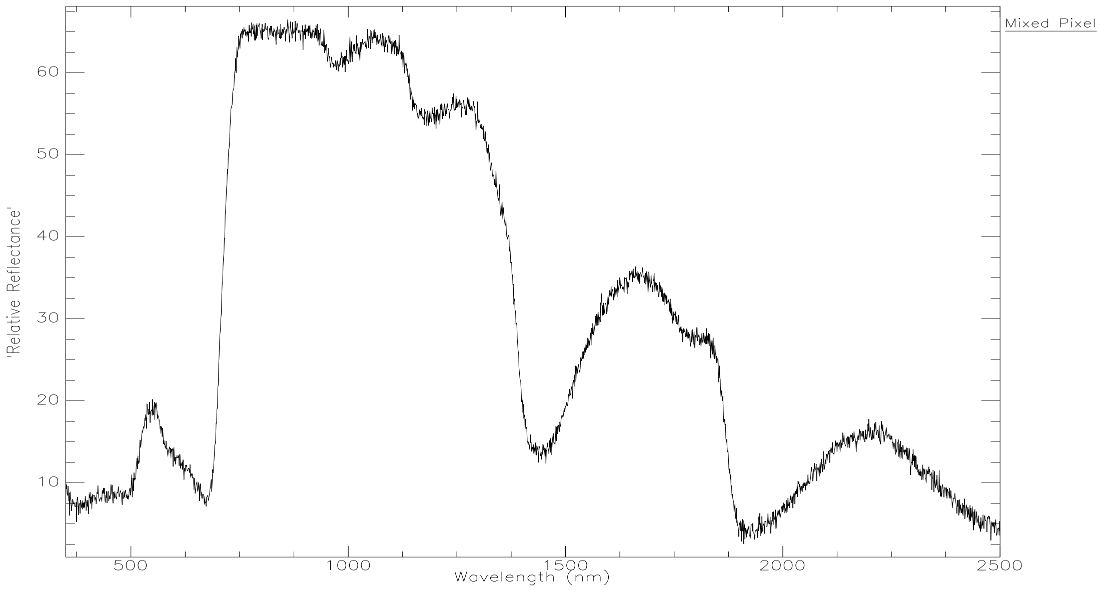

Figure 4.3: Mixed Pixel using Leafs Endmember (with noise)

The results of the second experiment are shown in the Table 4.2. The CLSPSTO algorithm converge faster to find the solution only in 3.42E-4 seconds, NNSTO and NNSTO are in the same order of magnitude. NNSTO took only 1 iteration average to converge. The time by iteration ISRA is the faster but ISRAA, EMML and EMMLA have the same order of magnitude (10^{-5}).

Table 4.2: Timing Results for Leafs HSI Data (with noise)

	EMML	ISRA	EMMLA	ISRAA	NNLS	CLSPSTO	NNSLO	NNSTO
Time (sec)	1.08E-1	9.49E-2	3.55E-2	5.51E-2	3.63E-3	**3.42E-4**	8.00E-4	6.84E-4
Avg.♯ Iterations	1.14E+3	1.45E+3	4.12E+2	9.25E+2	4	1.52	1.36	**1**
$\frac{Time(sec)}{Iterations}$	8.81E-5	**6.72E-5**	9.20E-5	6.83E-5	9.03E-4	2.18E-4	7.564E-4	6.836E-4

4.1.3 Experiment 3: Different Spectral Signature

The third experiment consists in abundance estimation using different spectral signatures. The endmember the spectral signature of heulandite GDS3, azurite WS316, actinolite NMNH80714 and ammonioalunite NMNH145596 was used. The spectral signature of the minerals used are shown in the Figure 4.4. The minerals endmembers data consist of 420 bands range from 0.3951-2.56nm. Similar to the first experiment, the same generated abundance vector was used, where ammonioalunite 0.12578, actinolite 0.134351, azurite 0.554631, heulandite 0.185238. The mixed pixel used for the experiment is shown in the Figure 4.5.

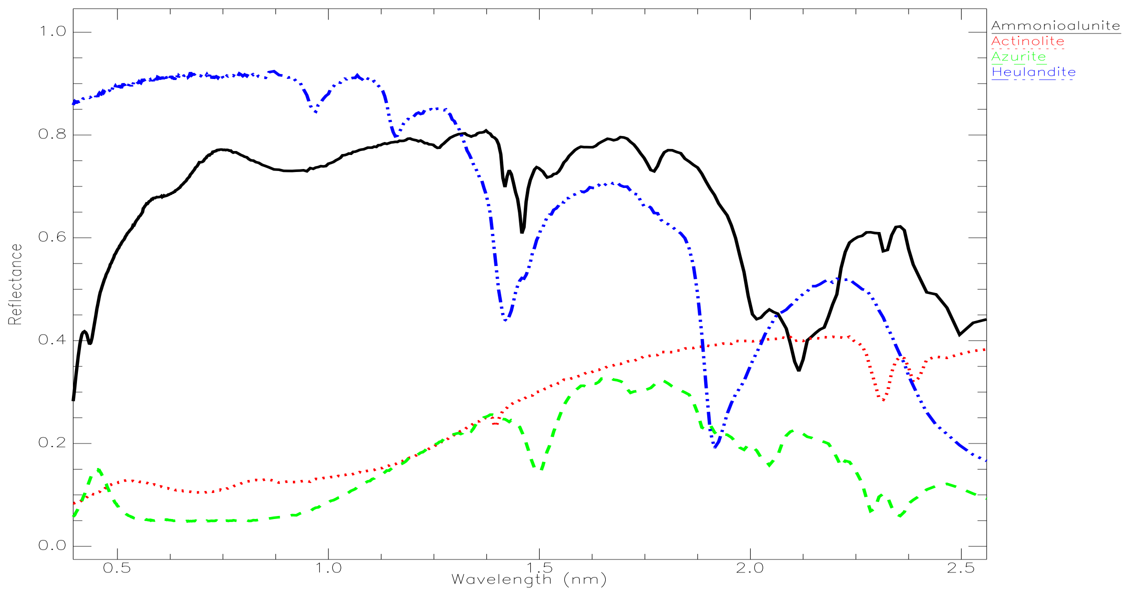

Figure 4.4: Minerals Endmembers

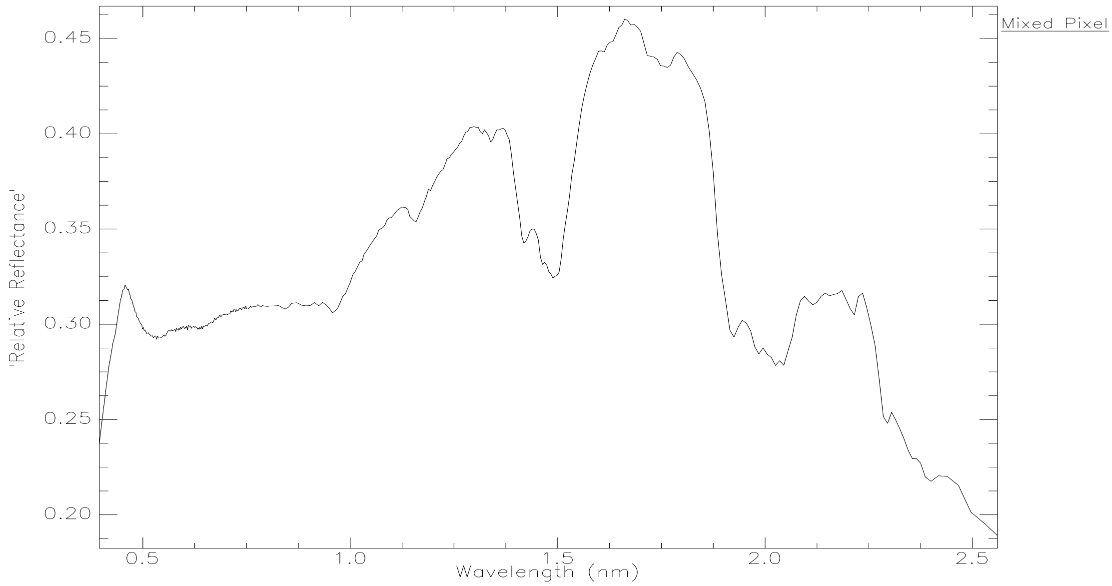

Figure 4.5: Mixed Pixel using Minerals Endmembers

The results of the third experiment are shown in the Table 4.3. In this experiment, the same pattern was observed that CLSPSTO converge faster than the other algorithms in only one iteration. In addition, NNSLO and NNSTO are in the same order of magnitude and took only one iteration. The EMMLA took less time by iteration but EMML, ISRA and CLSSTO are in the same order of magnitude.

Table 4.3: Unmixing Results for Minerals HSI Data

	EMML	ISRA	EMMLA	ISRAA	NNLS	CLSPSTO	NNSLO	NNSTO
Time (sec)	2.17E-2	5.45E-3	7.21E-3	1.42E-3	2.42E-3	**2.51E-4**	6.68E-4	8.40E-4
Avg.♯ Iterations	3.24E+2	8.36E+1	1.10E+2	1.88E+1	4	**1**	**1**	**1**
$\frac{Time(sec)}{Iterations}$	6.84E-5	5.93E-5	**5.44E-5**	2.19E-4	6.06E-4	2.51E-4	6.68E-4	8.40E-4

4.1.4 Experiment 4: Different Spectral Signature with Noise

The fourth experiment consist in adding noise to the minerals mixed pixel to estimate de abundances. The noise added is Gaussian Noise with N(0,α^2I) where α is the 1 percent of $max_i|b_i|$ (of the mineral mixed pixel). The mixed pixel with noise is shown in the Figure 4.6.

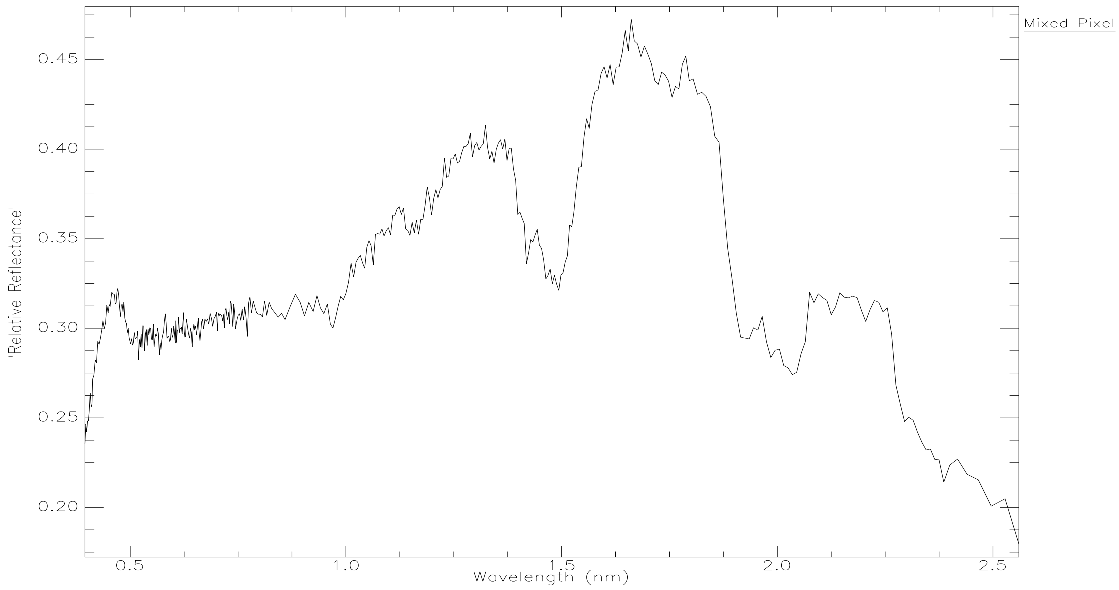

Figure 4.6: Mixed Pixel using Minerals Endmember (with noise)

Table 4.4: Unmixing Results for Minerals HSI Data with Noise

	EMML	ISRA	EMMLA	ISRAA	NNLS	CLSPSTO	NNSLO	NNSTO
Time (sec)	4.03E-2	3.18E-2	6.22E-3	1.04E-2	2.93E-3	**8.56E-5**	1.71E-4	9.95E-4
$Avg.\sharp$ $Iterations$	6.10E+2	6.15E+2	9.67E+1	1.91E+2	4	**1**	**1**	**1**
$\frac{Time(sec)}{Iterations}$	7.35E-5	**5.50E-5**	5.52E-5	5.71E-5	7.31E-4	8.56E-5	1.711E-4	9.947E-4

The Table 4.4 shown the results of this experiment. The same behavior in CLSPSTO was observed, faster convergence and only one iteration to converge, in addition, NNSLO and NNSTO converge only in one iteration. This case EMML, EMMLA, ISRA, ISRAA and CLSPSTO have the same order of magnitude (around 10^{-5}).

4.2 Experiments with Real Data: Enrique Reef

In this section, results of applying the abundance estimation algorithms described in Chapter 2 to real data taken with the Hyperion sensor [9] over Enrique Reef in La Parguera Puerto Rico are presented. The Enrique Reef is part of the La Parguera in southwest coast of Puerto Rico in the Municipality of Lajas. The Figure 4.7 shows an aerial photo of La Parguera. The Enrique Reef data used for this experiment consists of first 92 bands

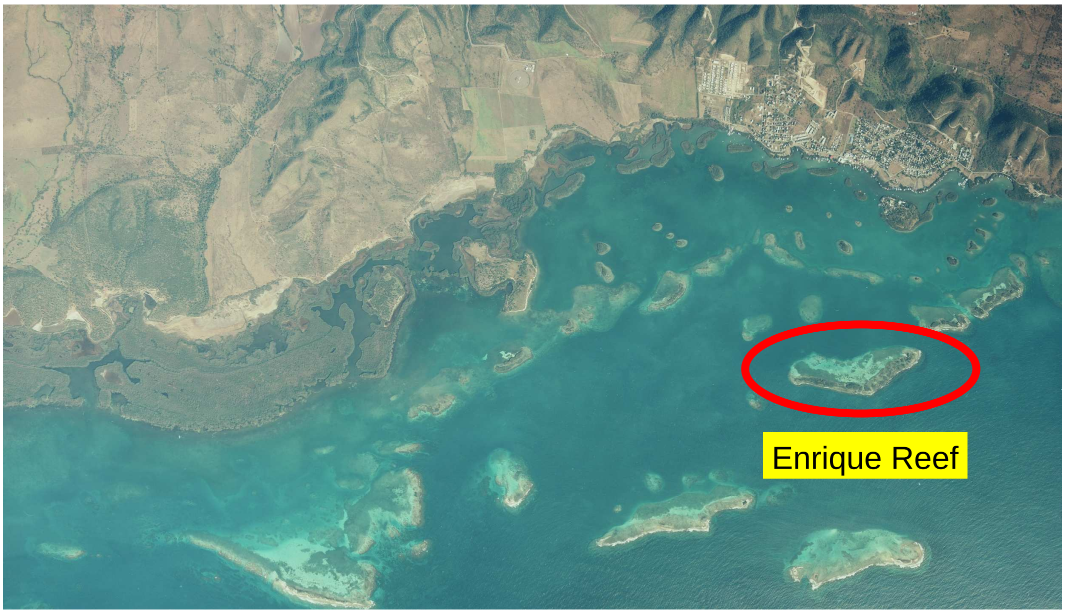

Figure 4.7: La Parguera: Lajas, PR

(of Hyperion sensor) from 435-890nm with a spatial resolution of 30 meters. The data was pre processed with Fast Line-of-sight Atmospheric Analysis of Spectral Hypercubes (**FLAASH**) [16] to remove atmospheric effects in the data. Figure 4.8 shows a color composite using Hyperion data of Enrique Reef. For experiments comparison, a high resolution image (1m) taken by the IKONOS sensor was used, is shown in Figure 4.9. The degradation cause by the low spatial resolution in Hyperion is clearly observed. In the Hyperion image, any of the spatial features are not easily to identify compare as IKONOS image. Figure 4.10 shows the classification map of Enrique Reef from done by Dr. Armstrong in 1982 [17]. In Figure 4.10, four objects of interest are identified: thalassia, reef flat, rhizophora and sand lagoon. The rest of the area of the image is deep sea water. The PPI method of ENVI to extract the endmembers from the Enrique Reef HSI data was used. The endmembers selected, sand, coral, rhizophora (mangrove), thalassia (sea grass) and water are shown in the Figure 4.11.

The results shown in the following sections, the images include an color bar indicating the range of values of the estimated abundances for each images. Red pixels color represent a greater abundance values and blue pixels color represent less abundance values. The residual images presented are estimated as follows: $\|\mathbf{A}\widehat{\mathbf{x}} - \mathbf{b}\|/\|\mathbf{b}\|$ where $\widehat{\mathbf{x}}$ is the abundance estimates of the different algorithms. Other results presented in this work is the summation of the estimated abundances to observe if the sum to one behavior in different pixels.

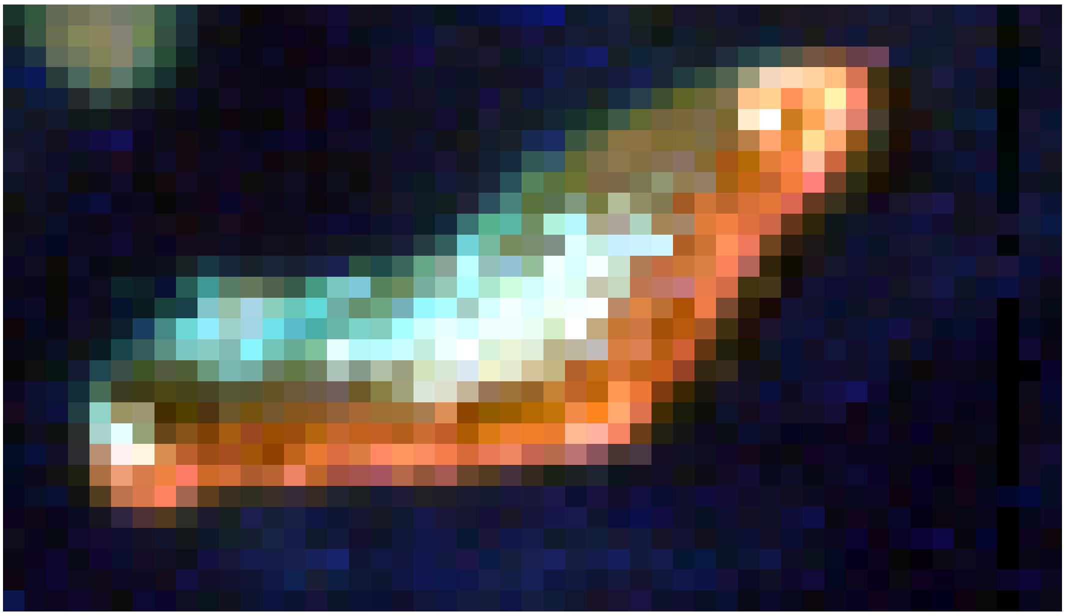

Figure 4.8: Enrique Reef Image from Hyperion HSI Sensor

4.2.1 Unconstrained Least Square Results

Figures 4.12-4.16 show the results for unconstrained least squares. The abundance estimates for water, coral and rhizophora (mangrove) are more closer visually to the IKONOS image. ULS results shown that negative abundance estimation are obtained also do not satisfy the sum to one constraints as shown in Figure 4.18. Most of the highest

Figure 4.9: Enrique Reef Image collected with IKONOS Sensor (1 meter resolution)

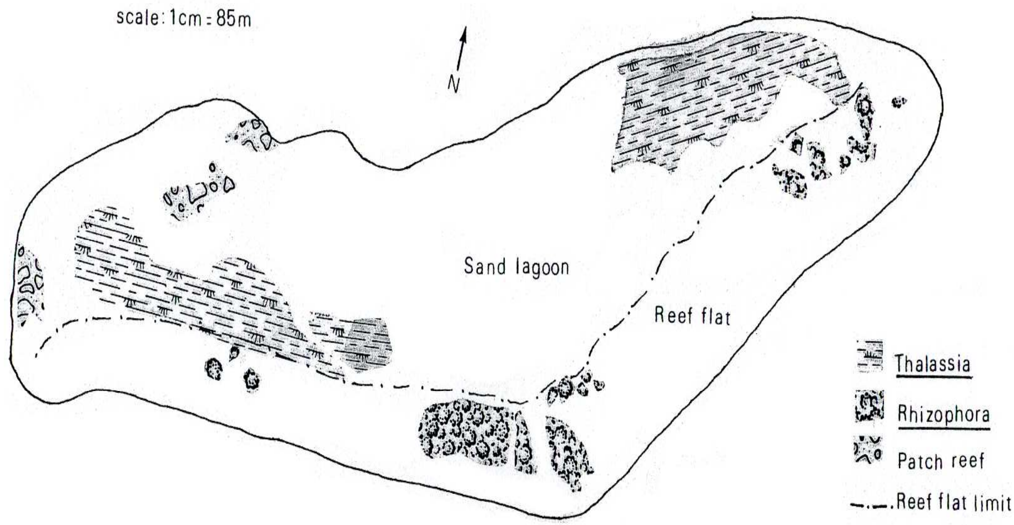

Figure 4.10: Classification Map of Enrique Reef

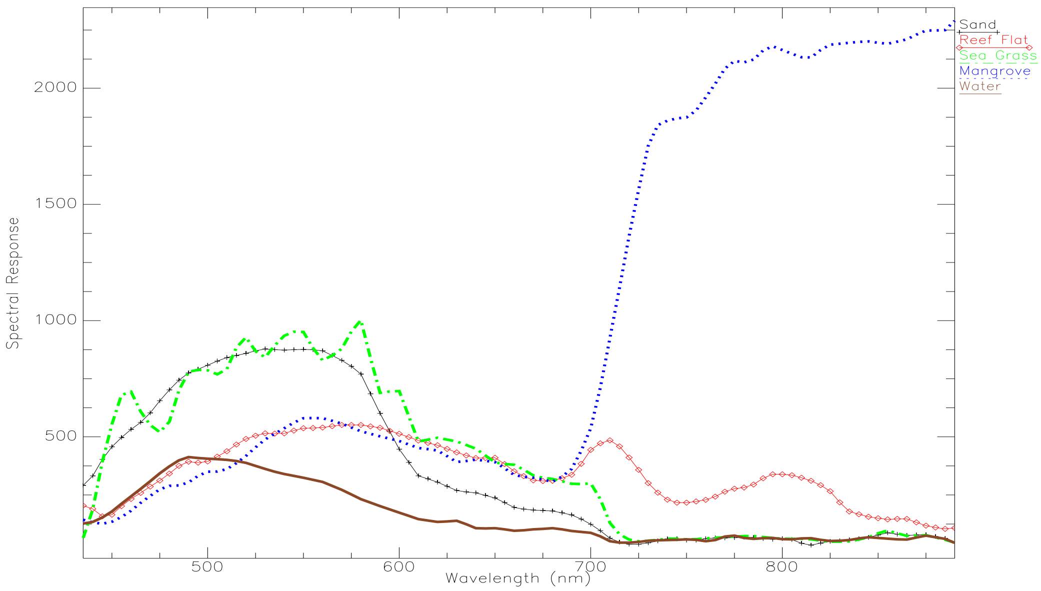

Figure 4.11: Enrique Reef Endmembers

residual estimates are from the water areas.

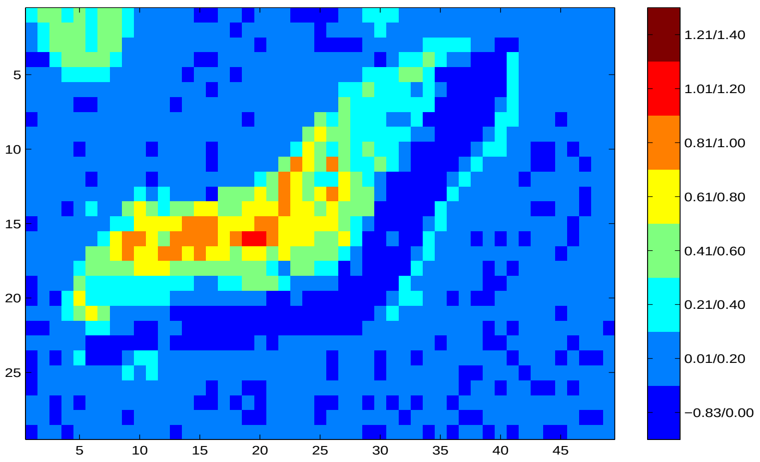

Figure 4.12: Sea Grass Abundance Estimates using ULS

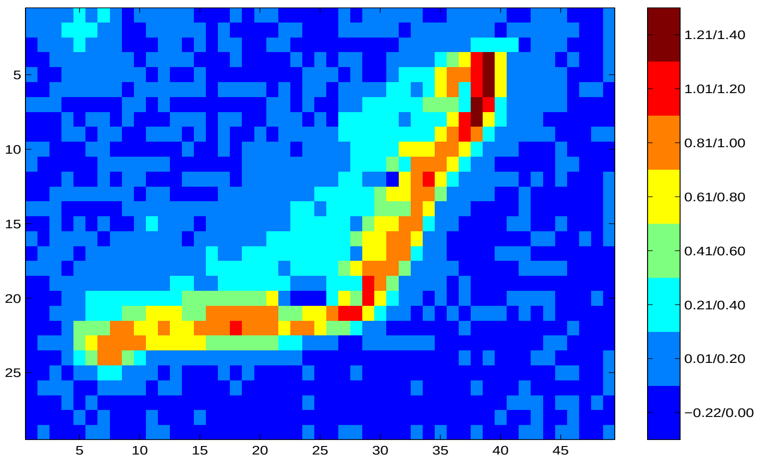

Figure 4.13: Coral Abundance Estimates using ULS

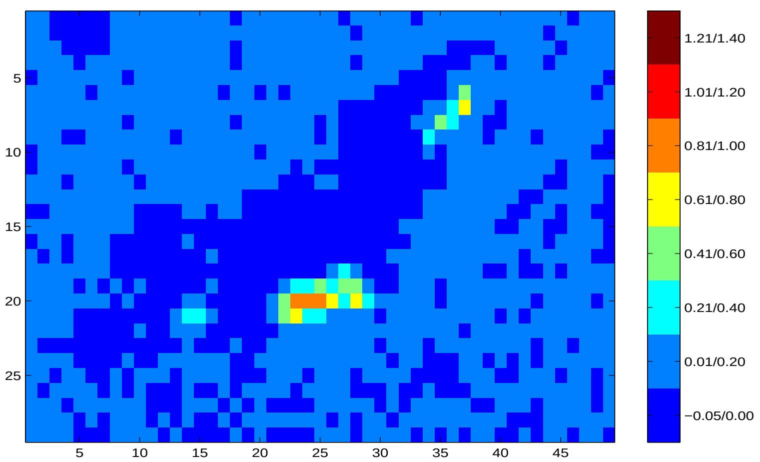

Figure 4.14: Mangrove Abundance Estimates using ULS

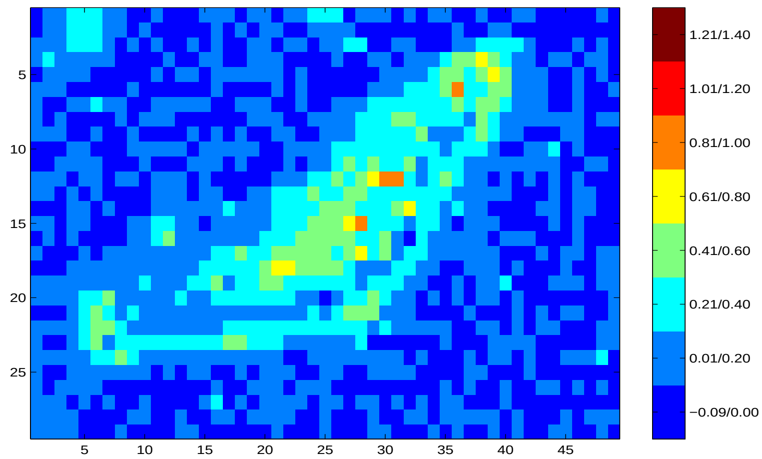

Figure 4.15: Sand Abundance Estimates using ULS

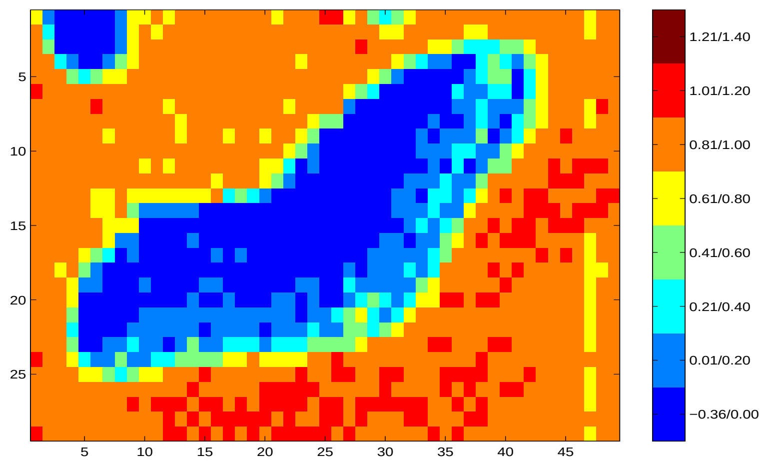

Figure 4.16: Water Abundance Estimates using ULS

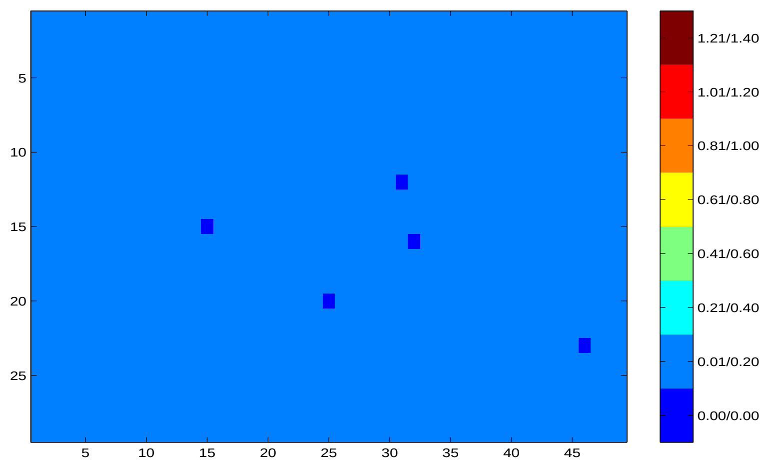

Figure 4.17: Residual Abundance Estimates using ULS

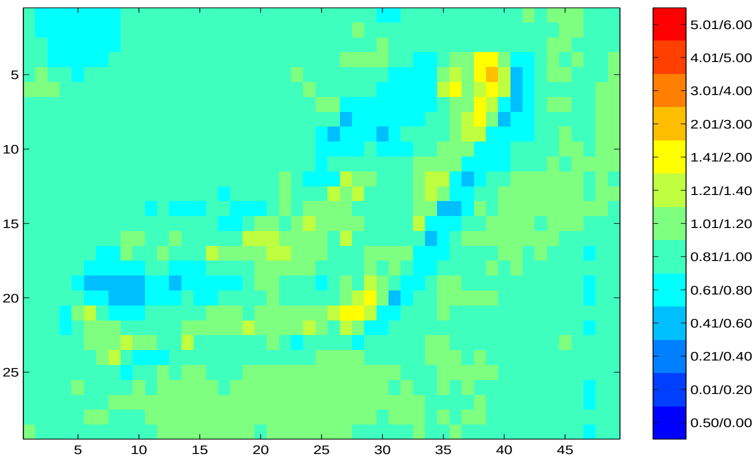

Figure 4.18: Summation of Abundance Estimates

4.2.2 Sum to One Least Square Results

This section shows the results obtained with the STOLS algorithm, the Figures 4.19 to 4.23 shown the abundance results. The results obtained in this experiment, only satisfy the sum to one constraints as shows Figure 4.25 but negatives abundance estimated values are obtained as are shown in Figure 4.20. In addition, the highest abundances residuals estimates are in the coral areas.

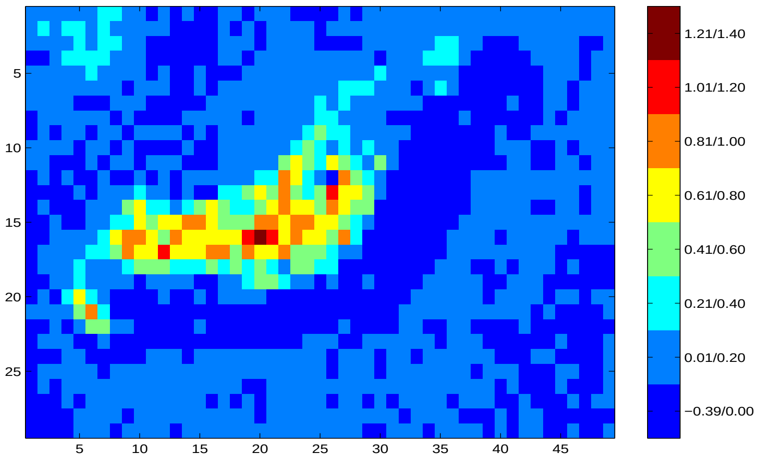

Figure 4.19: Sea Grass Abundance Estimates using STOLS

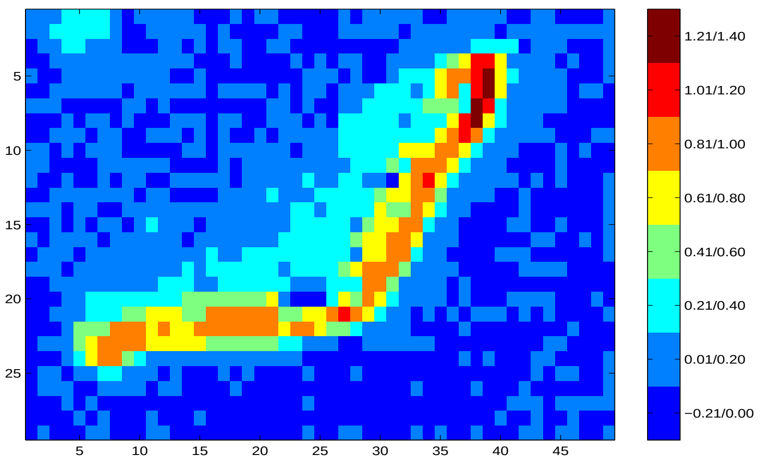

Figure 4.20: Coral Abundance Estimates using STOLS

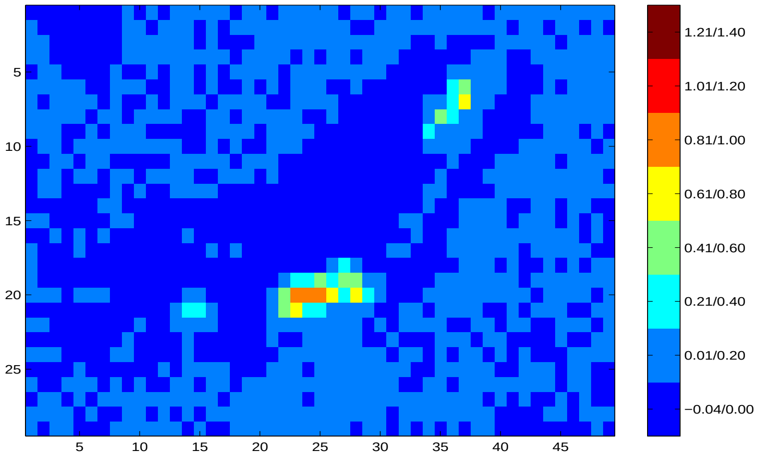

Figure 4.21: Mangrove Abundance Estimates using STOLS

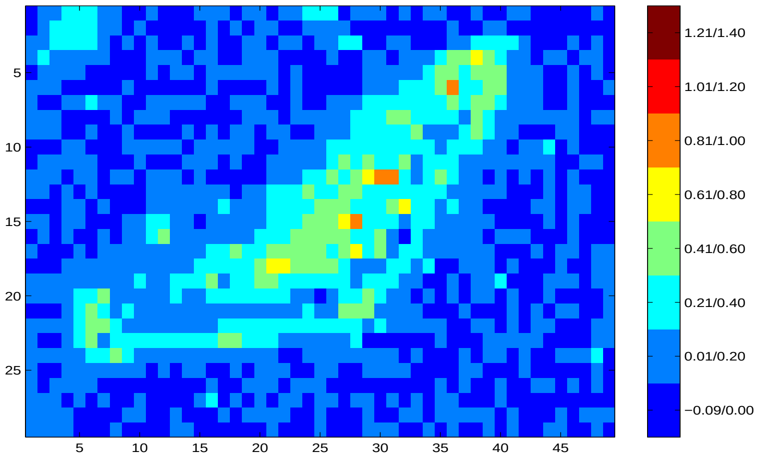

Figure 4.22: Sand Abundance Estimates using STOLS

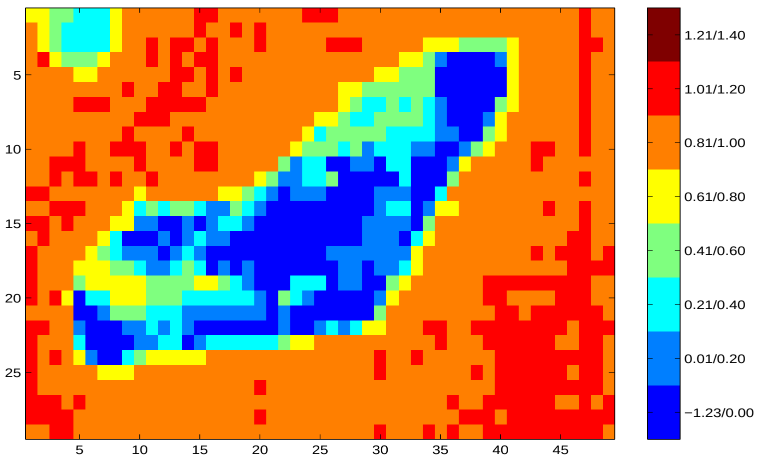

Figure 4.23: Water Abundance Estimates using STOLS

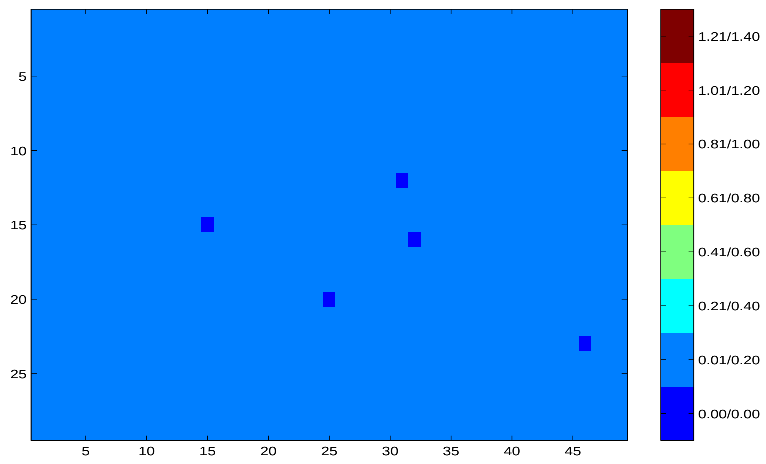

Figure 4.24: Residual Abundance Estimates using STOLS

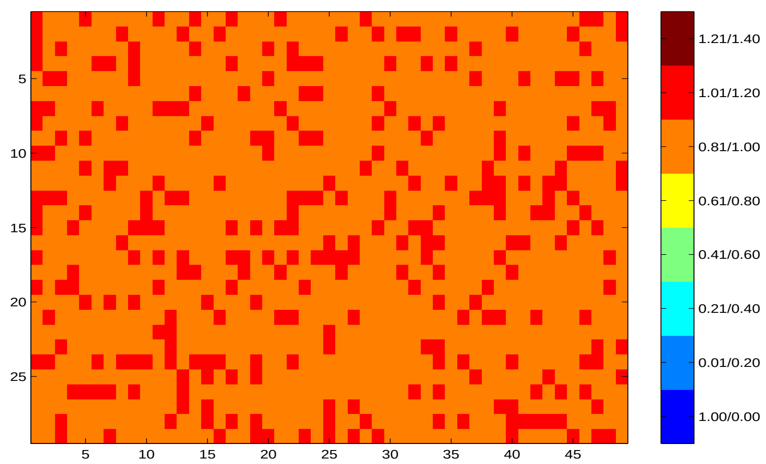

Figure 4.25: Summation of Abundance Estimates

4.2.3 EMML Results

The abundance estimates for the EMML algorithm are shown in the Figures 4.26 to 4.30. The results obtained shows a better definition in the coral, water and mangrove. In addition, the abundance estimates satisfy the nonnegative constraints. The highest residuals estimates where obtained in the coral and mangrove areas.

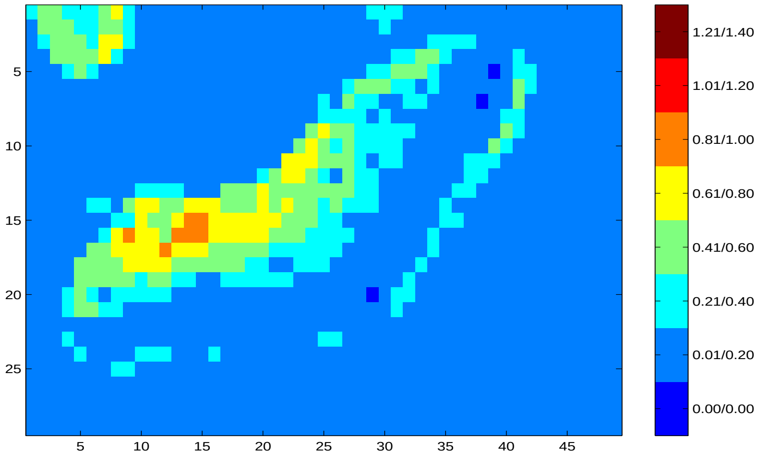

Figure 4.26: Sea Grass Abundance Estimates using EMML

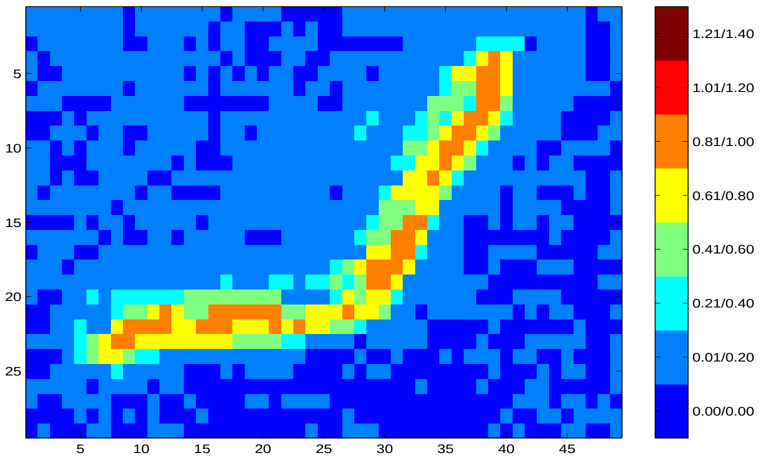

Figure 4.27: Coral Abundance Estimates using EMML

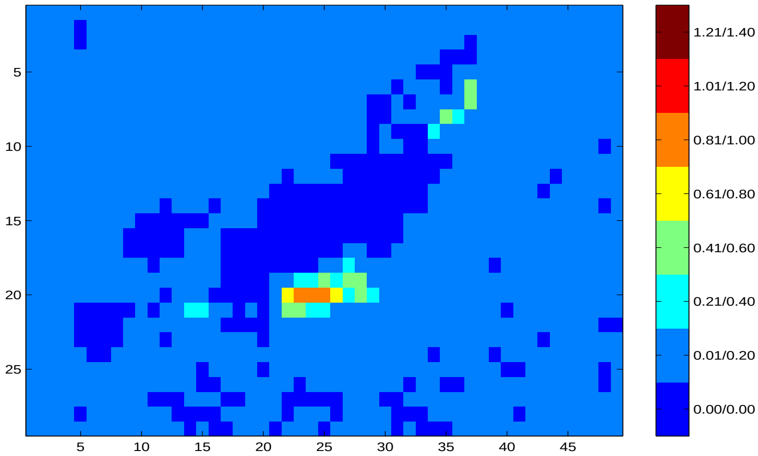

Figure 4.28: Mangrove Abundance Estimates using EMML

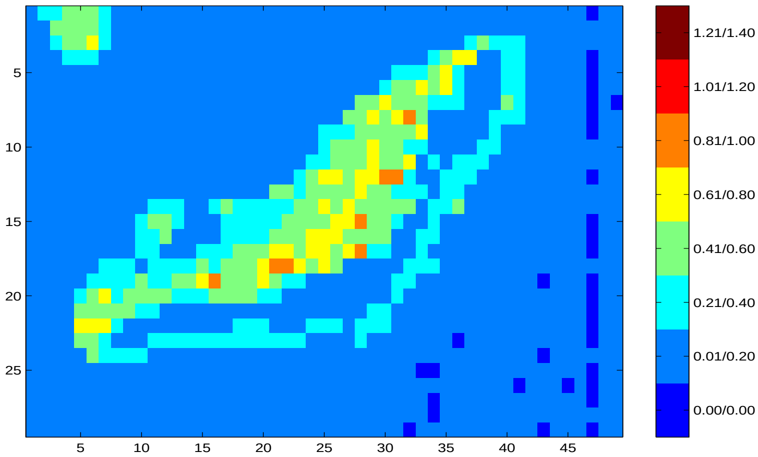

Figure 4.29: Sand Abundance Estimates using EMML

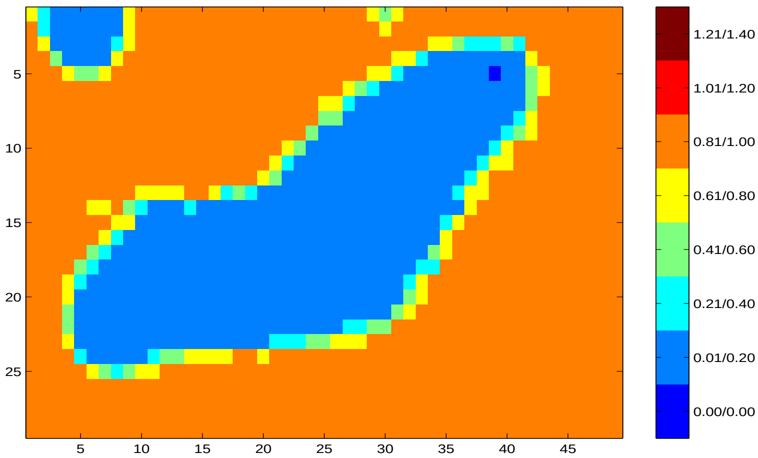

Figure 4.30: Water Abundance Estimates using EMML

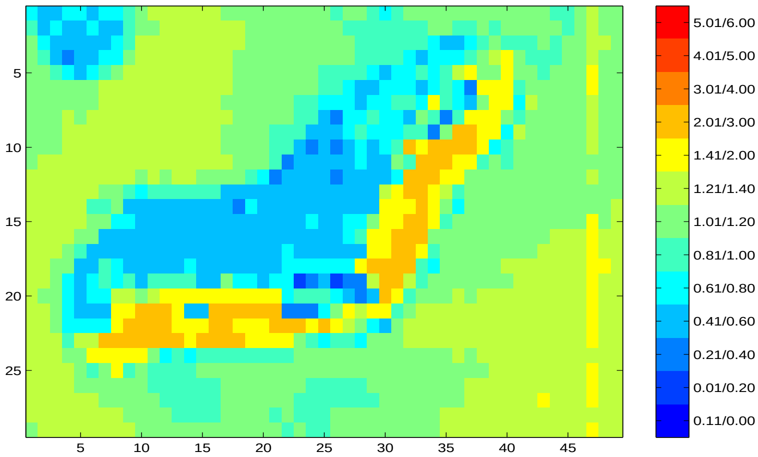

Figure 4.31: Residual Abundance Estimates using EMML

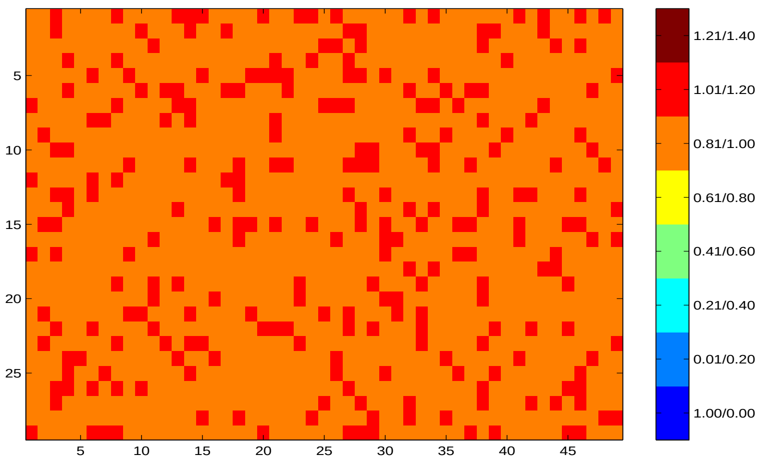

Figure 4.32: Summation of Abundance Estimates

4.2.4 ISRA Results

The abundance estimates for the ISRA algorithm are shown in the Figures 4.33 to 4.37. The results obtained with ISRA were similar to those of EMML. In the coral, mangrove and water abundance images, Figures 4.34, 4.35 and 4.37 are better distinguished in the corresponds area. In addition, the estimates satisfy the nonnegativity constraint. The residuals estimates obtained are similar to the ones obtained with EMML.

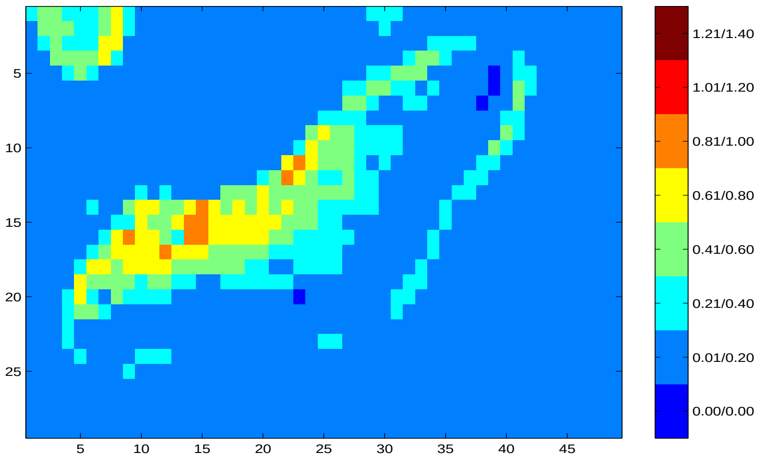

Figure 4.33: Sea Grass Abundance Estimates using ISRA

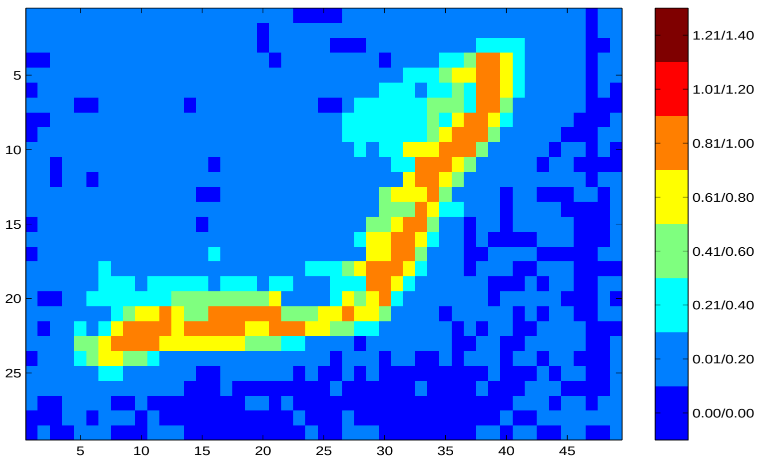

Figure 4.34: Coral Abundance Estimates using ISRA

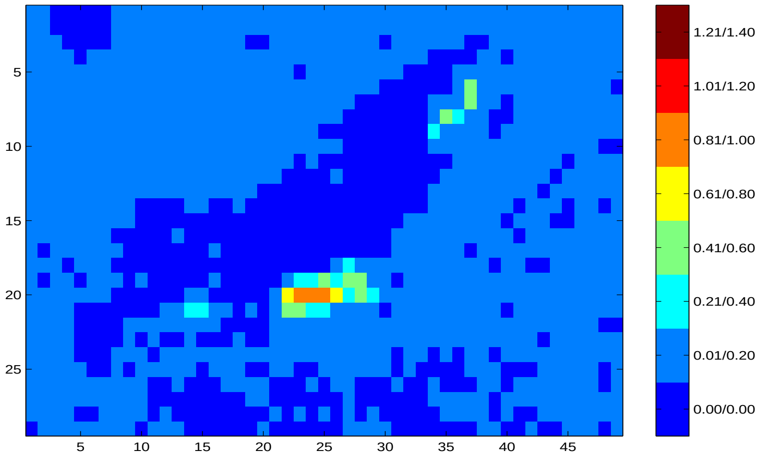

Figure 4.35: Mangrove Abundance Estimates using ISRA

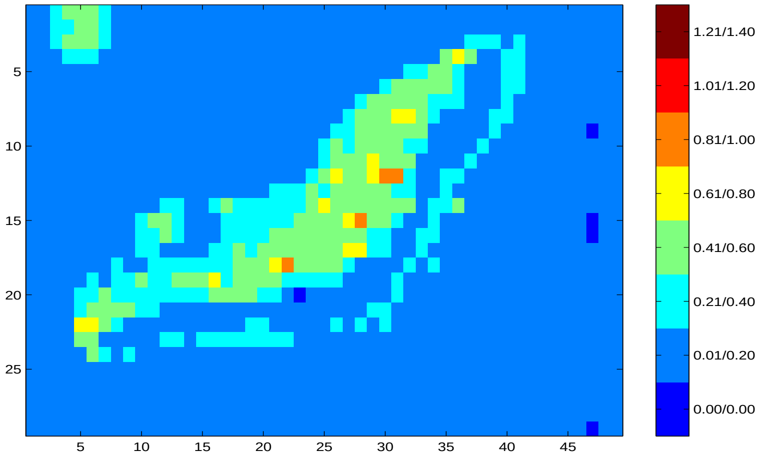

Figure 4.36: Sand Abundance Estimates using ISRA

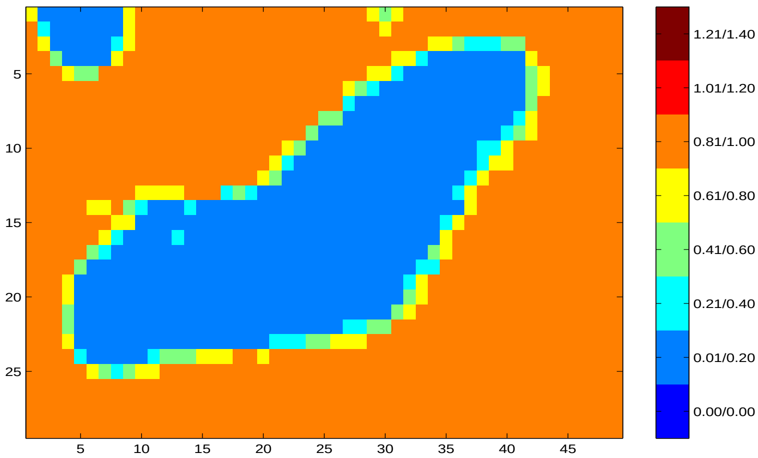

Figure 4.37: Water Abundance Estimates using ISRA

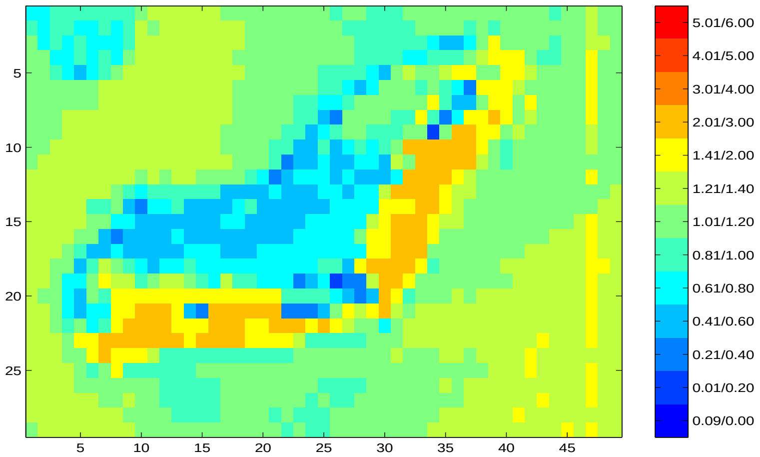

Figure 4.38: Residual Abundance Estimates using ISRA

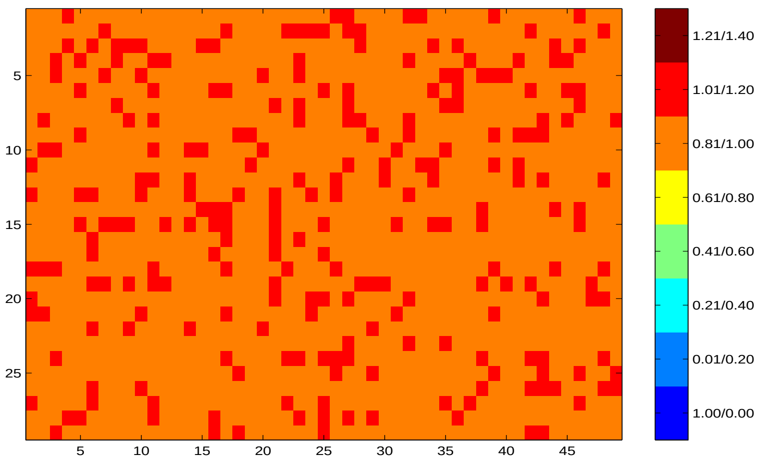

Figure 4.39: Summation of Abundance Estimates

4.2.5 NNLS Results

In this section, results for the NNLS algorithm for the Enrique Reef HSI Data are presented. The abundances estimates for sea grass, coral, mangrove, sand and water are shown in the Figures 4.40 to 4.44. The results obtained with NNLS are similar to those of EMML and ISRA. In the coral, mangrove and water abundance images, Figures 4.41, 4.42 and 4.44 are better distinguished similar to EMML and ISRA. In addition, the color bar of the abundance images shows the abundances obtained by the algorithm satisfy the nonnegative constraints also the residual estimates obtained with NNLS are similar to EMML and ISRA.

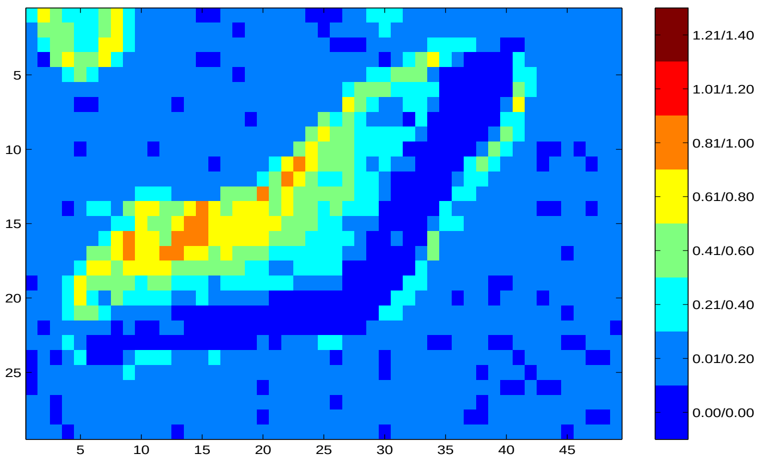

Figure 4.40: Sea Grass Abundance Estimates using NNLS

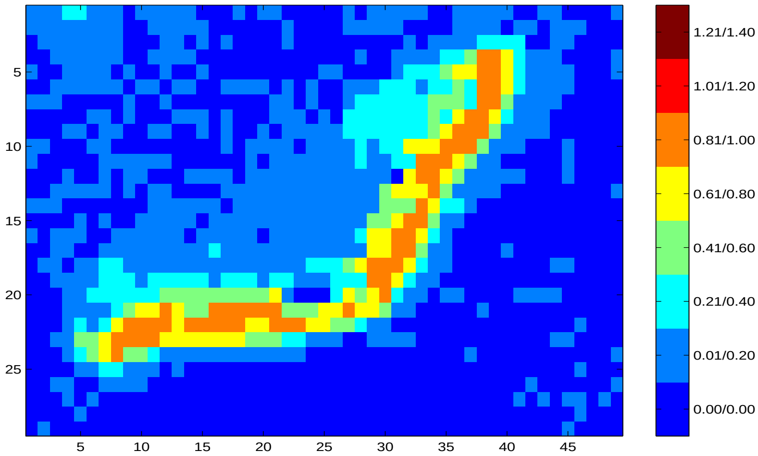

Figure 4.41: Coral Abundance Estimates using NNLS

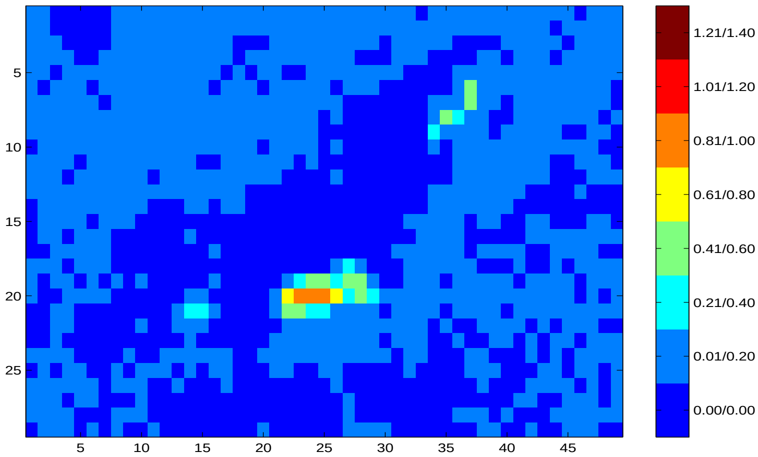

Figure 4.42: Mangrove Abundance Estimates using NNLS

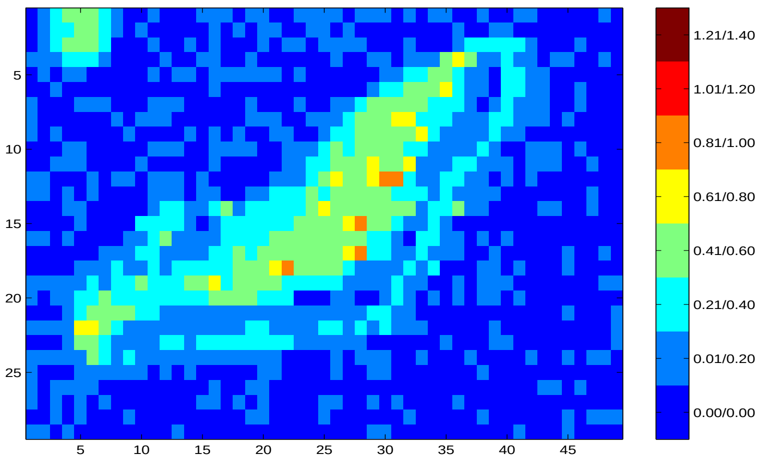

Figure 4.43: Sand Abundance Estimates using NNLS

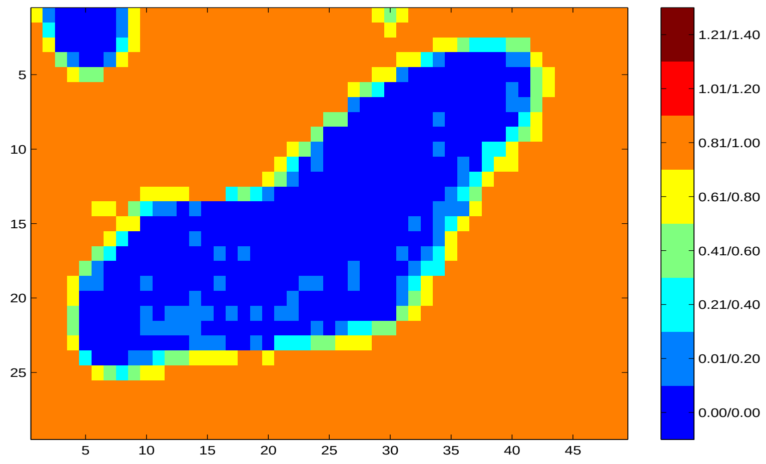

Figure 4.44: Water Abundance Estimates using NNLS

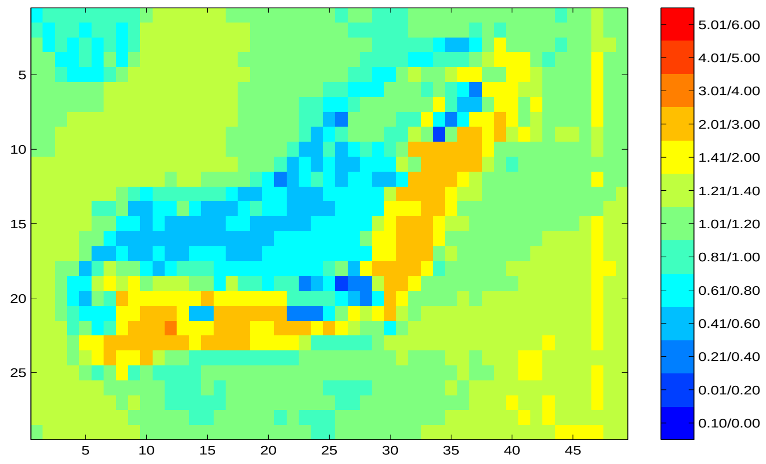

Figure 4.45: Residual Abundance Estimates using NNLS

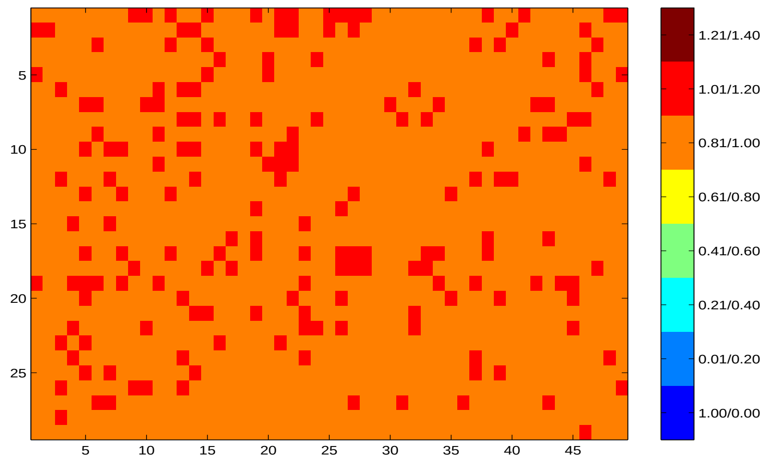

Figure 4.46: Summation of Abundance Estimates

4.2.6 CLSPSTO Results

The CLSPSTO abundances estimates are presented in this section. Figures 4.47 to 4.51 shows the abundances estimates of the Chang's algorithm [13]. Abundance estimates obtained for coral, Figure 4.48 and for mangrove, Figure 4.49 are similar to ISRA, EMML and NNLS. The sand (Figure 4.50 and sea grass (Figure 4.47 results are more similar to some of the areas of IKONOS image (Figure 4.9). Figure 4.50 of sand estimates and Figure 4.47 of sea grass are more likely to the IKONOS image. In addition, the abundance estimates that satisfy all the constraints.

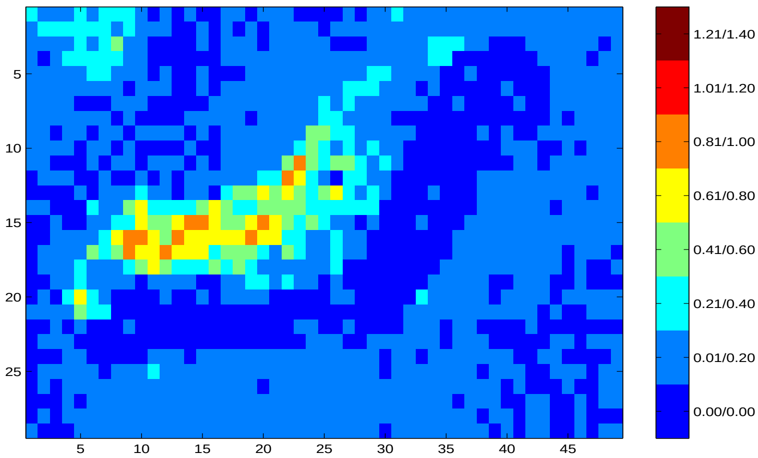

Figure 4.47: Sea Grass Abundance Estimates using CLSPSTO

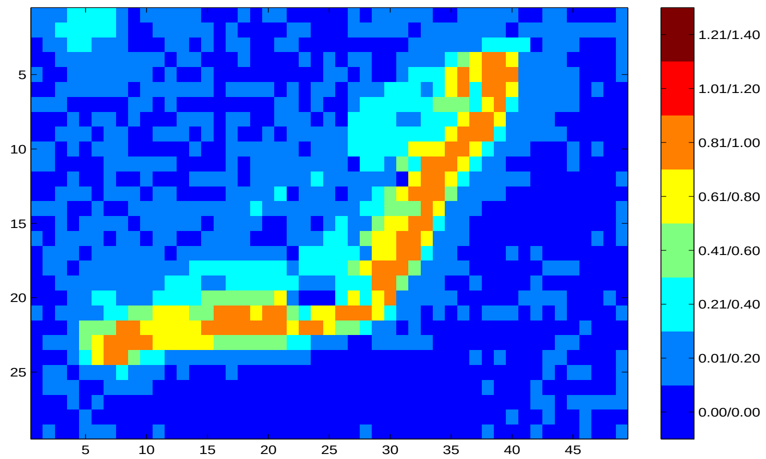

Figure 4.48: Coral Abundance Estimates using CLSPSTO

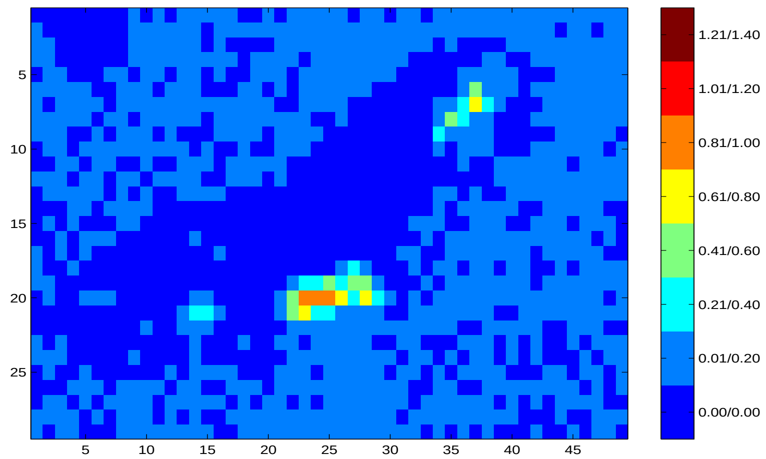

Figure 4.49: Mangrove Abundance Estimates using CLSPSTO

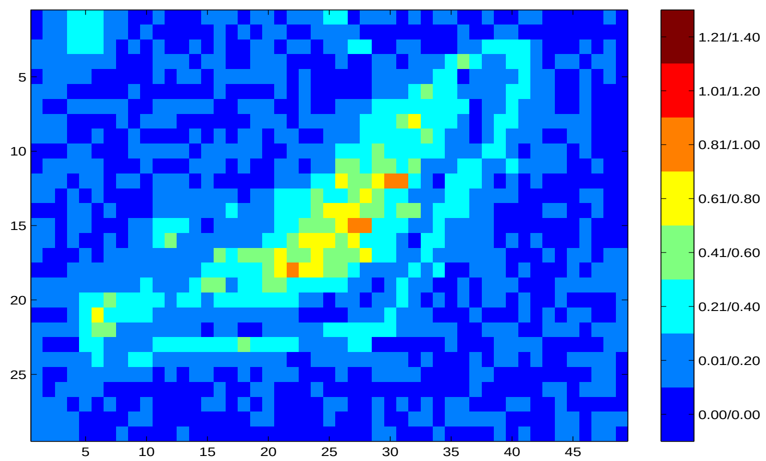

Figure 4.50: Sand Abundance Estimates using CLSPSTO

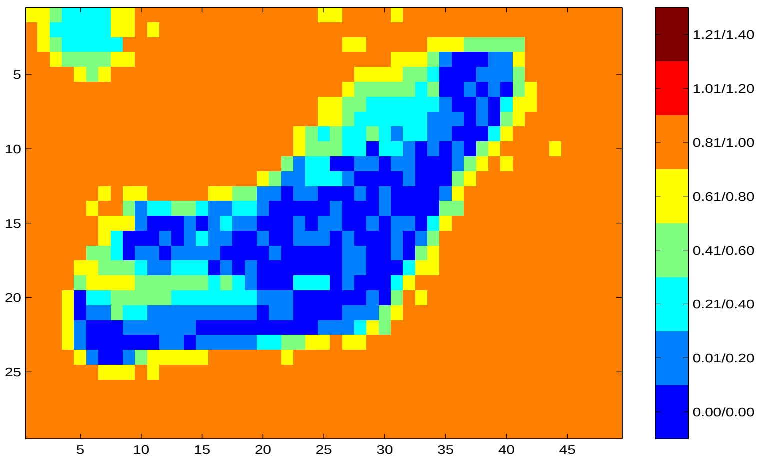

Figure 4.51: Water Abundance Estimates using CLSPSTO

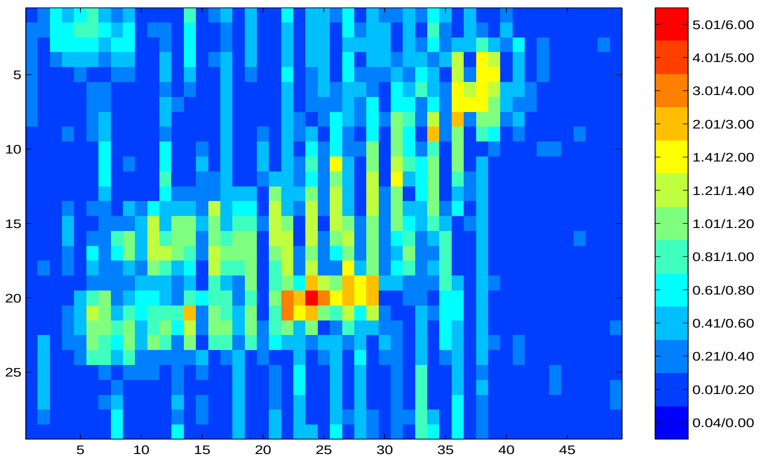

Figure 4.52: Residual Abundance Estimates using CLSPSTO

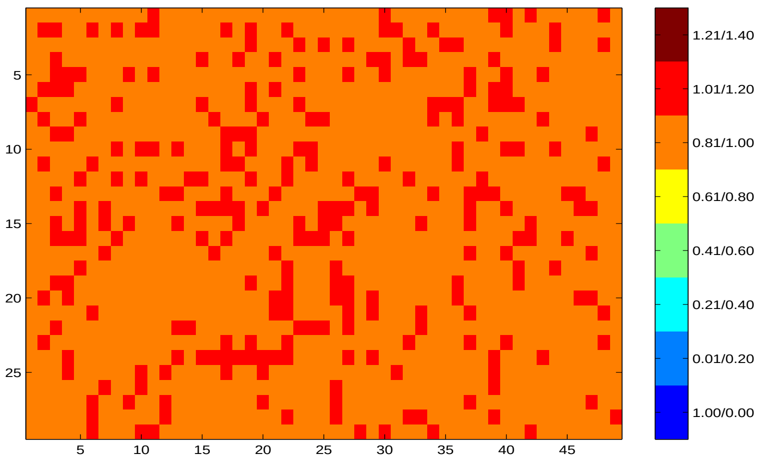

Figure 4.53: Summation of Abundance Estimates

4.2.7 NNSLO Results

In this section, the results for the NNSLO algorithm for the Enrique Reef HSI Data are shown. The abundances estimates for sea grass, coral, mangrove, sand and water are shown in the Figures 4.54 to 4.58. The abundance estimation objects are very similar to the areas of the IKONOS image. In addition, observing the images color bar the abundance estimates obtained by the algorithm satisfy the nonnegative constraints. Figure 4.60 shows the sum less or equal to one constraints, most of the areas of the image have values above 0.9, some cases values around 0.6 are observed most of this values are in the coral regions but we also observe some in the water and the sea grass.

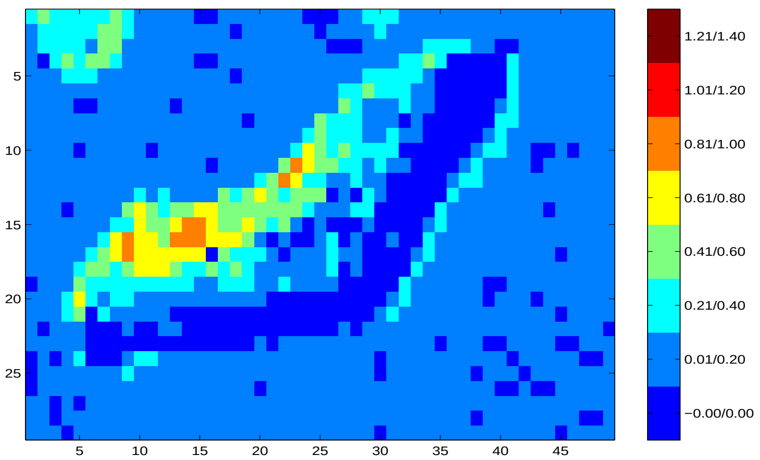

Figure 4.54: Sea Grass Abundance Estimates using NNSLO

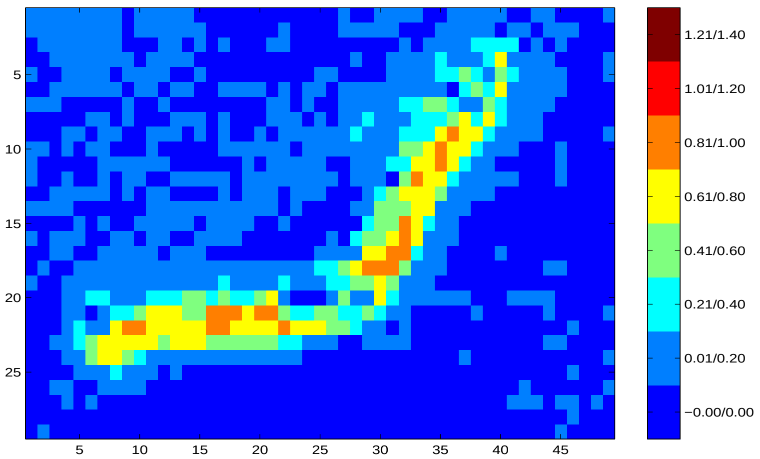

Figure 4.55: Coral Abundance Estimates using NNSLO

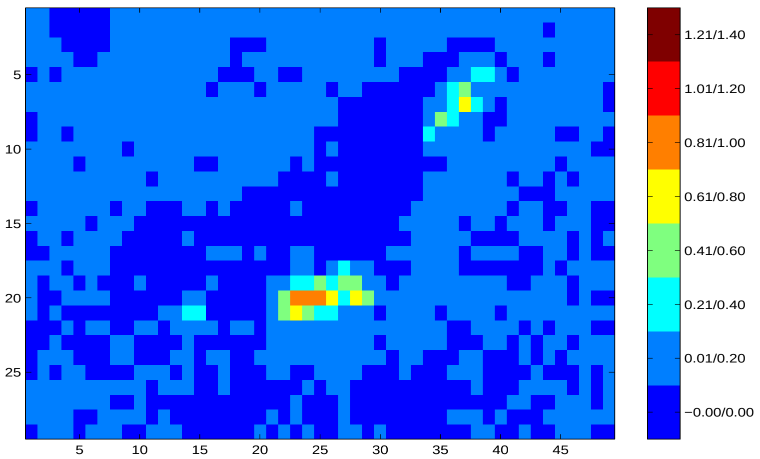

Figure 4.56: Mangrove Abundance Estimates using NNSLO

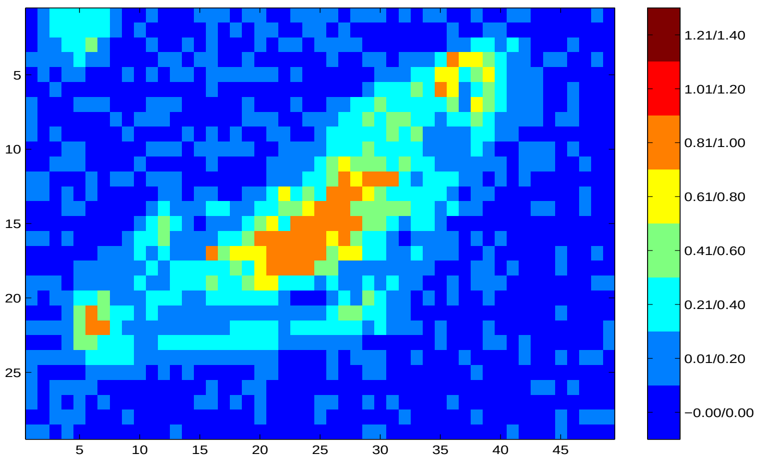

Figure 4.57: Sand Abundance Estimates using NNSLO

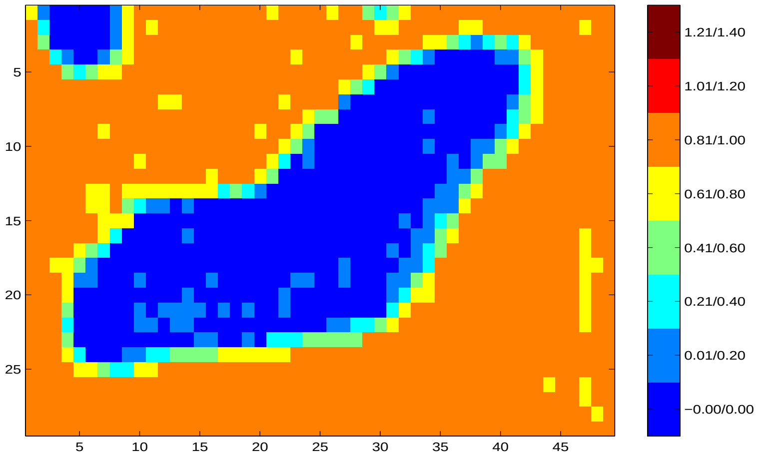

Figure 4.58: Water Abundance Estimates using NNSLO

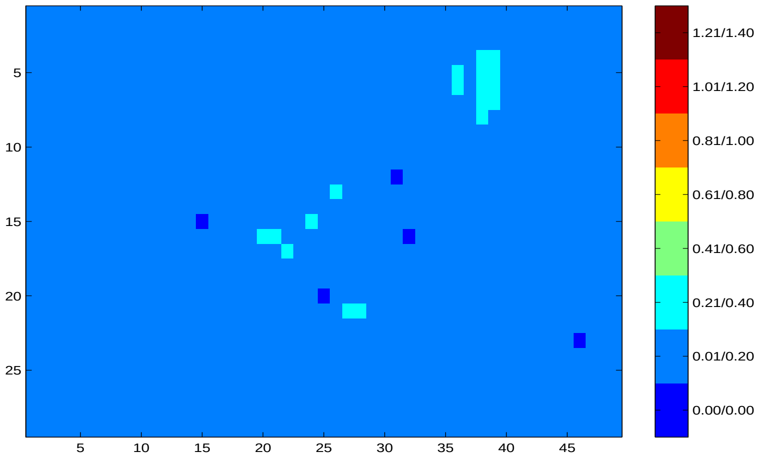

Figure 4.59: Residual Abundance Estimates using NNSLO

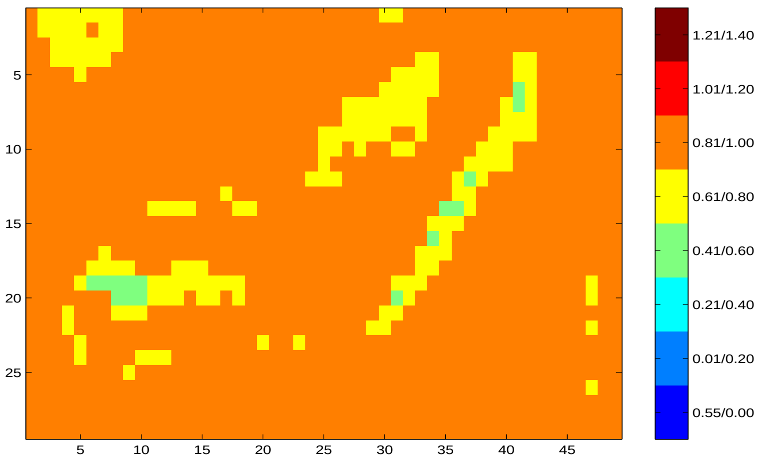

Figure 4.60: Summation of Abundance Estimates

4.2.8 NNSTO Results

In this section, the results for the NNSTO algorithm for the Enrique Reef HSI Data are presented. The abundances estimates for sea grass, coral, mangrove, sand and water are shown in the Figures 4.61 to 4.65. The abundance estimation of coral, mangrove and sea grass are very similar to the results of NNSLO. The estimation results of water and sand are more similar to IKONOS image. Similar to NNSLO, with NNSTO the algorithms obtains abundance estimates satisfying the nonnegative and the sum to one constrains as shown in Figure 4.67. In addition, the abundance residual estimates are similar to NNSLO.

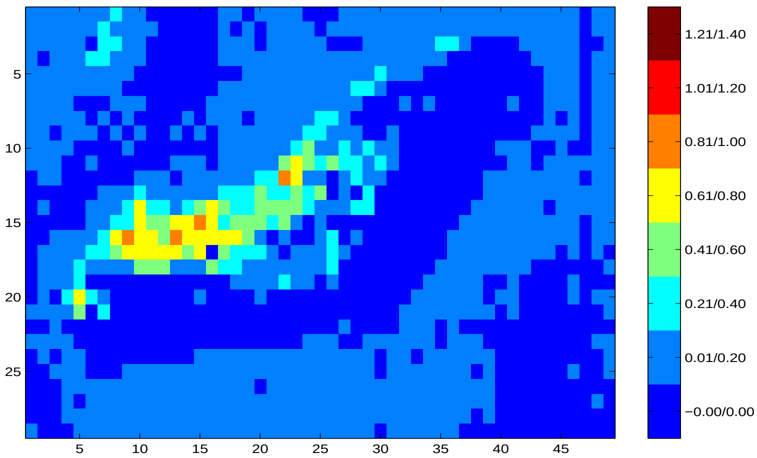

Figure 4.61: Sea Grass Abundance Estimates using NNSTO

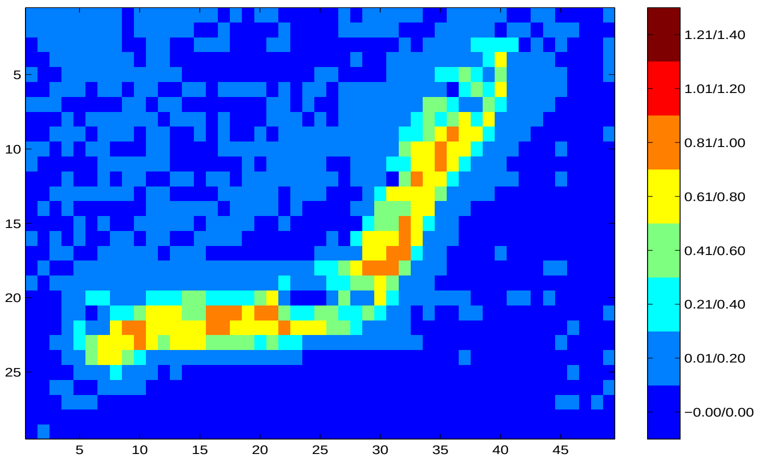

Figure 4.62: Coral Abundance Estimates using NNSTO

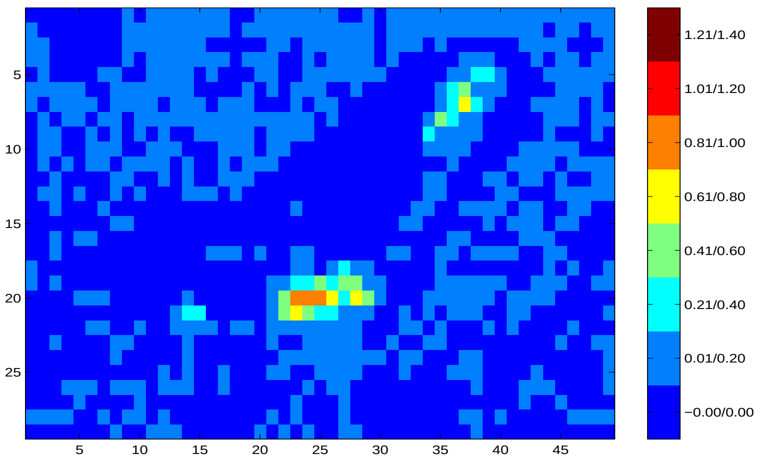

Figure 4.63: Mangrove Abundance Estimates using NNSTO

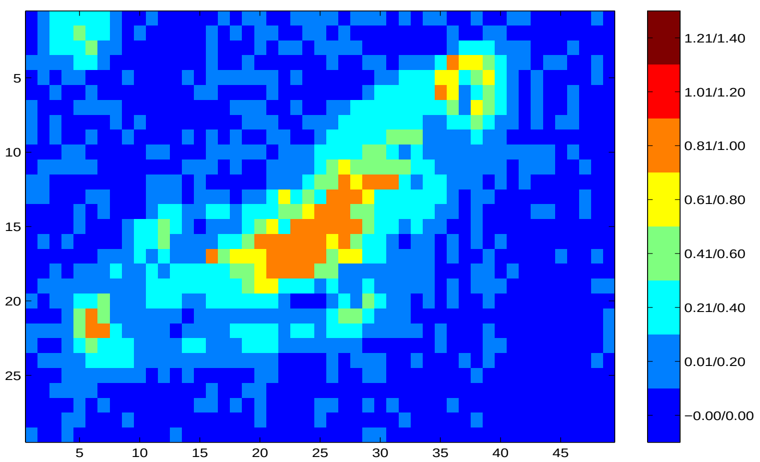

Figure 4.64: Sand Abundance Estimates using NNSTO

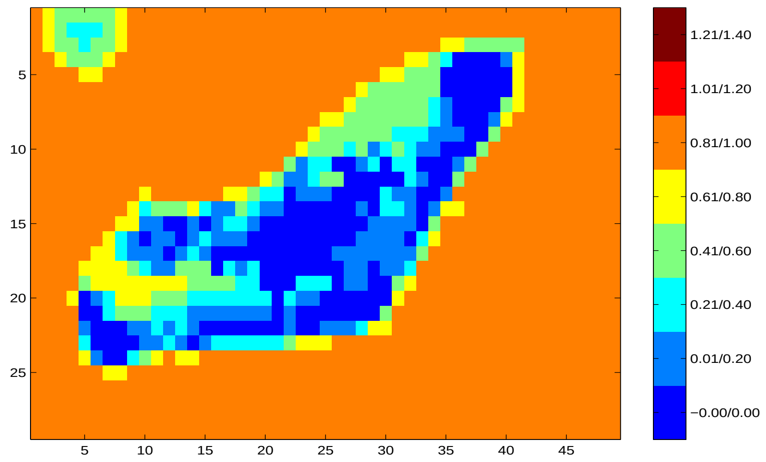

Figure 4.65: Water Abundance Estimates using NNSTO

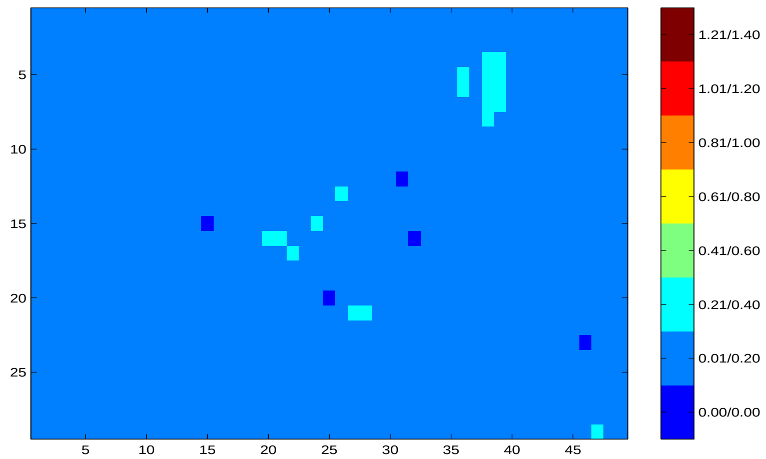

Figure 4.66: Residual Abundance Estimates using NNSTO

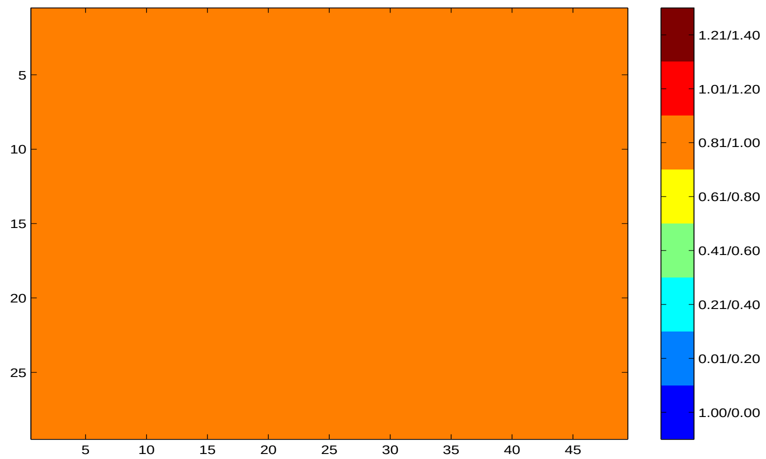

Figure 4.67: Summation of Abundance Estimates

4.3 Conclusions

In this Chapter, different experiments with synthetic and real data to study the behavior of the abundance estimation algorithms were presented. The synthetic experiment results showed that CLSPSTO algorithms converged faster than the other algorithms in one iteration (in most cases). In the test of time by iterations, ISRA algorithm run faster per iteration than the other algorithms in most cases.

Using the direct approaches, ULS and STOLS to solve the AEP does not produce abundance estimation with the desired constraints for the Enrique Reef HSI data. In general ISRA, EMML and NNLS produce similar abundance estimation results, the estimation for water, coral reef and mangrove agree visually with are similar to the IKONOS image. In addition, CLSPSTO, NNSLO and NNSTO produce good estimation of water, coral reef and mangrove. CLSPSTO produce a better abundance estimation of sea grass compared with ISRA, EMML and NNLS also NNSLO and NNSTO produce sea grass estimation closer to the IKONOS image. The abundance estimation results for sand obtained with NNSLO and NNSTO are more closer to IKONOS image than the results obtained with CLSPSTO. Also the results of NNSLO and NNSTO are very similar in the abundance estimation of coral reef, sea grass and mangrove this is because NNSTO is derived from NNSLO. NNSLO and NNSTO differs in the water and sand estimates. Water estimation with NNSTO it gives more weight in areas where are sand and sea grass than NNSLO.

CHAPTER 5

Conclusions and Future Work

The purpose of this work was to study the behavior of abundance estimator algorithms using synthetic and real HSI data. The integration of the non negative and sum to one or sum less than one constraints as part of the solutions for the abundance estimation problem have been presented in this work, as they are ISRA, NNLS, EMML and CLSPSTO. Two new algorithms to tackle the abundance estimation problem were presented: one considering dark pixels, sum less or equal to one and non negativeness constraints, NNSLO; another considering non negative and sum less or equal to one constraints NNSTO.

In this research, simulation experiments with synthetic HSI data to study the algorithm convergence behavior under controlled situations were performed. The results obtained of the experiments led to conclude that CLSPSTO is faster than the others algorithms (order of magnitude of 10^{-4}) and converge in one iteration in most cases. ISRA algorithm run faster per iteration than the others algorithms.

Based on the results obtained from the abundances estimation for Enrique Reef HSI data the algorithms with non negative and sum less or equal to one and non negative and sum to one, NNSLO, CLSPSTO and NNSTO respectively, agree visually with high resolution IKONOS image of the area. Considering the residual images presented, NNSLO and NNSTO algorithms obtained better estimation than CLSPSTO. Including the constraints in the abundance estimation problem, sum to one, sum less to one and non negative constraints provide a better abundance estimates in addition to the estimates have physical meaning.

5.1 Future Work

In this research, the abundances estimation problem a part of the unmixing problem was only address, this let to future work in the following topics to be studied:

- More experimentation with better ground truth for validation of the algorithms. Choosing better ground truth (endmembers) help us to have a better abundance estimation, in addition, of having a sample closer to the objects of the observed area.
- Abundance Estimation plus Endmember Estimation to solve the *Unmixing Problem*. Solving the Unmixing Problem with no a priori information has been an interesting problem, in addition of develop automatic algorithms to solve the unmixing problem with little human interaction.
- Convergence time: accelerations methods for faster convergence to perform real time unmixing. Having real time algorithms we can include in sensors for instantaneous unmixing estimations.
- Study of water effects of subsensing objects in hyperspectral images and removing the water column before running the abundances estimation algorithms.
- Image registration with ENVI/IDL to validate the results using images of IKONOS.

BIBLIOGRAPHY

[1] Vélez-Reyes M.; et. al. "Iterative Algorithms for Unmixing of Hyperspectral Imagery". *Proceeding of SPIE*, April 2003.

[2] Vélez Reyes M.; Jiménez L.O.; et. al. "Comparison of Matrix Factorization Algorithms for Band Selection in Hyperspectral Imagery". *In Algorithms for Multispectral, Hyperspectral and Ultraspectral Imagery VI, Proceedings of SPIE*, 4049, 2000.

[3] Keshava N.; Mustard J. F. "Spectral Unmixing". *IEEE Signal Processing Magazine*, 19:44 – 57, January issue 1 2002.

[4] Kruse F.A. "Visible-Infrared Sensor and Case Studies". *Remote Sensing for the Earth Sciences: Manual of Remote Sensing*, 3, 1999.

[5] Plaza A.; Martinez P.; et. al. "Spatial-spectral Endmember Extraction by Multidimensional Morphological Operations". *IEEE Transactions on Geosciences and Remote Sensing*, 9:2025 – 2041, September 2002.

[6] Boardman J.W. "Geometric Mixture Analysis of Imaging Sectrometry Data". *Geoscience and Remote Sensing Symposium*, 4:2369 – 2371, 1994.

[7] Lawson C. L. and Hanson R. J. *"Solving Least Square Problems"*. Prentice-Hall, Inc., 1974.

[8] Clark R. N. "Chapter 1: Spectroscopy of Rocks and Minerals, and Principles of Spectroscopy". *Manual of Remote Sensing*, pages 3 – 58, 1999.

[9] Kruse F.A.; Boardman J.W.; Huntington J.F.; Mason P.; Quigley M.A. "Evaluation and Validation of EO-1 Hyperion for Geologic Mapping". *IEEE International Geoscience and Remote Sensing Symposium, 2002.*, 1:593 – 595, 2002.

[10] Shepp L.A.; Vardi Y. "Maximum Likelihood Reconstruction for Emission Tomography". *In IEEE Transactions on Medical Imaging*, MI-1(2), October 1982.

[11] Meidunas E.; Puetz A.; et. al. "RBI-EMML Separation for Imaging Techniques". *Proceedings of SPIE*, 4725, 2002.

[12] Daube-Witherspoon M. E.; Muehllehner G. "An Iterative Image Space Reconstruction Algorithm Suitable for Volume ECT". *In IEEE Transactions on Medical Imaging*, June 1986.

[13] Chang C. I.; Ren H.; et. al. "Subpixel Target Size Estimation for Remotely Sensed Imagery". *Proceedings of SPIE*, pages 398 – 407, 2003.

[14] Luenberger D. G. *"Linear and Nonlinear Programming"*. Addison-Wesley Publishing CO, second edition edition, 1984.

[15] Bjorck A. "Numerical Methods for Least Squares Problems". *SIAM, Amsterdan*, 1996.

[16] Cooley T.; et. al. "FLAASH, a MODTRAN4-based Atmospheric Correction Algorithm, its Application and Validation". *Geoscience and Remote Sensing Symposium, 2002. IGARSS '02. 2002 IEEE International*, June 2002.

[17] Armstrong R. A. "Changes in Cayo Enrique, La Parguera, Puerto Rico, from 1936 to 1980 using Aerial Photoanalysis". *Thesis (M.S.) University of Puerto Rico, Mayagëz Campus*, 1981.